MODELLING AND EFFICIENT NUMERICAL METHOD FOR ION TRANSPORTS IN LIQUIDS UNDER ELECTROMAGNETIC INFLUENCE

XIANMIN XU*, XIAODI ZHANG †, AND WEIYING ZHENG‡

Abstract. In this paper, we propose a mathematical model to describe ion transports in liquid solution under the effect of electromagnetic fields, which is a coupled system of the Navier-Stokes equations, the Nernst-Planck equations and the Maxwell equations. We show that the coupled system possesses an energy-dissipative structure while also preserving several important physical properties. We then develop a novel decoupled numerical method for the system by integrating well-designed implicit-explicit discretization for the nonlinear coupling terms, incorporating additional stabilization terms, and utilizing structure-preserving finite element pairs for the Navier-Stokes equations and the Maxwell equations. This method is very efficient, as it requires solving the Nernst-Planck equation for each ion concentration, the electric field equation, the magnetic field equation, and the Navier-Stokes equations separately at each time step. We prove that the fully discrete scheme exhibits several important properties: it conserves mass, maintains positivity, preserves magnetic flux, and is unconditionally energy stable. Numerical examples are given to verify the theoretical results.

Key words. Naver-Stokes-Nernst-Planck-Maxwell system; physics-preserving; finite element method; decoupled; energy stability.

AMS subject classifications. 65N12, 65M12, 65M70.

1. Introduction.

Electromagnetic fields are widely used in our daily life, which may also affect biological systems in many aspects. In particular, recent studies have investigated the direct effects of electromagnetic fields on neuronal ion channels [15, 5]. These investigations include experiments conducted on live animals [1, 12, 28, 35] as well as molecular dynamics simulations [31, 25]. The experiments examine different types of electromagnetic fields across a range of frequencies, from extremely low-frequency to radio-frequency and terahertz frequencies. However, the findings of these studies vary widely and even present controversies in certain aspects [5]. Consequently, there is a growing interest in exploring the interactions between electromagnetic fields and ion transport within ion channels in greater detail.

In the literature, the Navier-Stokes-Poisson-Nernst-Planck system is a widely used electrokinetic model for studying the dynamics of electrically charged fluids, including the motion of ions and their interactions with electric fields and the surrounding fluid (see [40, 36, 46, 7, 8] among many others). In this system, the Navier-Stokes equations describe the dynamics of incompressible fluids, the Nernst-Planck equations characterize ion transport and diffusion, and the Poisson equation addresses the electric potential. However, since the Poisson equation primarily models static electric fields, it is inadequate for capturing the effects of dynamic electromagnetic fields. In this work, we focus on ion transport within ion channels influenced by electromagnetic fields [5, 31]. Therefore, we propose a continuum model that consists of a coupled Navier-Stokes-Nernst-Planck-Maxwell system (see Equ. (2.12)). The system is designed to address three distinct physical processes: the Navier-Stokes equations for fluid dynamics, the Nernst-Planck equations for ion transport and diffusion, and the Maxwell equations for electromagnetic fields. Beyond its potential applications in biology, this system can also be used to describe fluid motion at the nanoscale, where the interactions between ions and fluid dynamics are critical [2, 27].

There already exists many mathematical studies on systems with two of the three physical processes in charged fluids. For example, the well-posedness of a coupled system of the Navier-Stokes equations and the Poisson-Nernst-Planck equations has been studied in [40, 46, 8, 9]. The coupled system of the Navier-Stokes equations and the Maxwell equations has also been analyzed theoretically in [17, 4, 3]. Numerically, the Navier-

*LSEC, Academy of Mathematics and Systems Science, Chinese Academy of Sciences, Beijing, 100190, China. School of Mathematical Science, University of Chinese Academy of Sciences, Beijing 100049, China. (xmxu@lsec.cc.ac.cn)

†Corresponding Author. School of Mathematics and Statistics, Zhengzhou University, Zhengzhou 450001, China. (zhangxiaodi@lsec.cc.ac.cn)

‡LSEC, Academy of Mathematics and Systems Science, Chinese Academy of Sciences, Beijing, 100190, China. School of Mathematical Science, University of Chinese Academy of Sciences, Beijing 100049, China. (zwy@lsec.cc.ac.cn)

Stokes-Poisson-Nernst-Planck equations have been extensively studied recently, e.g. in [36, 22, 13, 10, 23, 7], where different finite element methods have been adopted to solve the system. Optimal convergence rate is proved in [36, 13] for the nonlinear fully implicit schemes. The coupled system of an inviscid Navier-Stokes equation and the Maxwell equations has been solved by conservative Riemann solvers in [43]. In addition, some structure-preserving schemes are proposed for a Maxwell-Ampère-Nernst-Planck model in [38, 39] where the possion equation for the electric potential is replaced by the Maxwell-Ampère equation for the electric displacement [37]. In comparison to the previous studies, the Navier-Stokes-Nernst-Planck-Maxwell system with three coupled physical processes will be much more complicated to analyze and to solve numerically.

We try to develop a decoupled numerical scheme for the Navier-Stokes-Nernst-Planck-Maxwell system (2.12) which preserves the physical properties as much as possible. We prove that the system (2.12) preserves positivity and the total mass for each ion concentration, preserves the magnetic flux and also has an energy dissipative structure. To design efficient numerical scheme for the multi-physics system, we take several important strategies. Firstly, we keep the term $\sum_{i=1}^{m} \hat{\alpha}\nabla c_i$ in the first equation of (2.12), which has been absorbed in the pressure term in the literature(e.g [40, 7, 8, 22, 13]). The strategy seems nothing special, but it is important in getting rid of the exactly divergence-free condition for the velocity, which is essensial to prove the energy stability in the previous methods [7, 13]. Then we do a log transformation to ion density function c_i in the system, which helps on preserve the positivity for the ion concentrations. Based on the transformed model, we further design a decoupled fully discrete numerical scheme by choosing proper implicit-explicit discretization for the nonlinear coupling terms, incorporating additional stabilization terms, and utilizing structure-preserving finite element pairs for the Navier-Stokes equations and the Maxwell equations. In each time step, we need only to solve the Navier-Stokes equations, the Nernst-Planck equations and the Maxwell equations sequentially, which can be solved efficiently by standard numerical techniques. Moreover, the computations of magnetic field and the electric field are also decoupled, and the concentrations of each ion can be solved separately. We prove that the decoupled fully discrete scheme preserves the positivity and the total mass for each component of the ions, preserves the magnetic flux, and also keeps the same energy stability structure as that for the continuous problem. Numerical experiments verify the theoretical results and also show that our method has optimal convergence rates for the velocity, the concentration, the pressure and the magnetic fields. In addition, the decoupled numerical scheme can be used to solve some interesting three dimensional problems efficiently.

The rest of the paper is organized as follows. In Section 2, we develop the mathematical model and do non-dimensionalization to the system. We also prove some key properties of the system, including the positivity and the mass conservation for the ion concentration, the divergence free property for the magnetic field, and the energy dissipation structure. We develop a decoupled fully discrete numerical scheme for the model in Section 3. In Section 4, we prove that the numerical scheme preserves the key physical properties for the continuous problem shown in Section 2. Some numerical examples are given to verify the theoretical result and to test the convergence in Section 5. Finally, we give some concluding remarks in Section 6.

2. The mathematical models.

In this section, we first derive a mathematical model for charge transport and fluid motion for incompressible electrolyte solution under electromagnetic fields. Then we investigate some key properties of the model.

2.1. Model derivation.

Consider an electrolyte solution composed of m species of ions within a bounded and connected domain $\Omega \subset \mathbb{R}^3$ that has a Lipschitz continuous boundary $\Gamma := \partial\Omega$. We begin by introducing the governing equations for the fluid motion of the solution. We assume that the solution is an incompressible, homogeneous, Newtonian fluid with a constant density ρ and a constant dynamic viscosity η. At a given point $\boldsymbol{x}$ in space and time t, the fluid's velocity and pressure are denoted by $\boldsymbol{u}(\boldsymbol{x}, t)$ and $p(\boldsymbol{x}, t)$, respectively. For the i-th species ($i = 1, \cdots, m$), let $c_i(\boldsymbol{x}, t)$ be its ion concentration, z_i be its valency and $\boldsymbol{v}_i(\boldsymbol{x}, t)$ be its average velocity. It is well-known that when the velocity of the ions is inconsistent with the velocity of the electrolyte solution, the ions have a friction effect on the motion of the fluid [20]. In the range of linear response, we can assume that the friction force is proportional to the relative velocity, $f_i = \xi_i c_i(\boldsymbol{v}_i - \boldsymbol{u})$, where ξ_i is the friction coefficient of the i-th type of ions with respect to the solution. Thus, we model the incompressible flow by the

following Navier-Stokes equations,

$$\rho\left(\frac{\partial \boldsymbol{u}}{\partial t}+\boldsymbol{u}\cdot\nabla\boldsymbol{u}\right)-\eta\Delta\boldsymbol{u}+\nabla p=\sum_{i=1}^{m}\xi_i c_i\left(\boldsymbol{v}_i-\boldsymbol{u}\right), \tag{2.1}$$

$$\mathrm{div}\boldsymbol{u}=0. \tag{2.2}$$

Next, we consider the motion of ions in the solution. The concentration of the ions satisfies the mass conservation law,

$$\frac{\partial c_i}{\partial t}+\nabla\cdot(c_i\boldsymbol{v}_i)=0,\quad i=1,2,\cdots,m. \tag{2.3}$$

These equations are also referred to as continuity equations. For the average velocity $\boldsymbol{v}_i(\boldsymbol{x},t)$, we use the following constitutive relation,

$$\xi_i c_i(\boldsymbol{v}_i-\boldsymbol{u})=-\alpha\nabla c_i+c_i z_i\boldsymbol{E}+c_i z_i\boldsymbol{v}_i\times\boldsymbol{B}, \tag{2.4}$$

where α stands for the diffusion coefficient, $\boldsymbol{E}$ is the electric field and $\boldsymbol{B}$ is the magnetic induction. Physically, the above equation describes the balance of forces. The left-hand side of equation (2.4) represents the negative resistance of the fluid to the movement of ions, while the right-hand side denotes the driving force. This driving force encompasses the generalized force associated with diffusion processes, the force exerted by the electric field, and the Lorentz force resulting from the magnetic field.

Finally, the electromagnetic fields are described by the standard Maxwell equations,

$$\nabla\times\boldsymbol{E}+\frac{\partial\boldsymbol{B}}{\partial t}=\boldsymbol{0}, \tag{2.5}$$

$$\frac{1}{\mu_0}\nabla\times\boldsymbol{B}-\varepsilon_0\frac{\partial\boldsymbol{E}}{\partial t}=\sum_{i=1}^{m}c_i z_i\boldsymbol{v}_i, \tag{2.6}$$

$$\varepsilon_0\nabla\cdot\boldsymbol{E}=\sum_{i=1}^{m}c_i z_i, \tag{2.7}$$

$$\nabla\cdot\boldsymbol{B}=0. \tag{2.8}$$

Note that the charge density contributed by the i-th ion is $c_i z_i$, and the summation of then, $\sum_{m}^{i=1}c_i z_i$ is called net charge. Since the last two equations (2.7)-(2.8) can be deduced from (2.3) and (2.5)-(2.6), we will omit them in the remainder of the paper.

To summarize, we obtain the Navier–Stokes-Nernst-Planck-Maxwell (NSNPM) system as follows,

$$\rho\left(\frac{\partial \boldsymbol{u}}{\partial t}+\boldsymbol{u}\cdot\nabla\boldsymbol{u}\right)-\eta\Delta\boldsymbol{u}+\nabla p=\sum_{i=1}^{m}\xi_i c_i(\boldsymbol{v}_i-\boldsymbol{u}), \tag{2.9a}$$

$$\mathrm{div}\boldsymbol{u}=0, \tag{2.9b}$$

$$\frac{\partial c_i}{\partial t}+\nabla\cdot(c_i\boldsymbol{v}_i)=0,\qquad i=1,2,\cdots,m, \tag{2.9c}$$

$$-\alpha\nabla c_i+z_i\boldsymbol{E}+c_i z_i\boldsymbol{v}_i\times\boldsymbol{B}=\xi_i c_i(\boldsymbol{v}_i-\boldsymbol{u}),\qquad i=1,2,\cdots,m, \tag{2.9d}$$

$$\nabla\times\boldsymbol{E}+\frac{\partial\boldsymbol{B}}{\partial t}=\boldsymbol{0}, \tag{2.9e}$$

$$\frac{1}{\mu_0}\nabla\times\boldsymbol{B}-\varepsilon_0\frac{\partial\boldsymbol{E}}{\partial t}=\sum_{i=1}^{m}c_i z_i\boldsymbol{v}_i. \tag{2.9f}$$

2.2. Nondimensionalize and simplification. We now deduce the dimensionless form for the system (2.9) and make some simplifications.

Let $L, t_0, B_0, E_0, c_0, z_0, u_0 = L/t_0$ be characteristic quantities of length, time, magnetic field, electric field, ion concentration, charge and fluid velocity, respectively. We introduce the dimensionless variables as follows

$$\begin{aligned} &\boldsymbol{x} \leftarrow \boldsymbol{x}/L, \quad t \leftarrow t/t_0, \quad \boldsymbol{u} \leftarrow \boldsymbol{u}/u_0, \quad p \leftarrow p/\left(\rho u_0^2\right), \\ &c_i \leftarrow c_i/c_0, \quad z_i \leftarrow z_i/z_0, \quad \boldsymbol{B} \leftarrow \boldsymbol{B}/B_0, \quad \boldsymbol{E} \leftarrow \boldsymbol{E}/E_0. \end{aligned}$$

Let c be the speed of light, when we assume that $E_0 = B_0\mathrm{c}$, the system (2.9) can be written in a dimensionless form as,

$$\frac{\partial \boldsymbol{u}}{\partial t} + \boldsymbol{u}\cdot\nabla\boldsymbol{u} - R_e^{-1}\Delta\boldsymbol{u} + \nabla p = \sum_{i=1}^{m} f_{r,i}c_i(\boldsymbol{v}_i - \boldsymbol{u}), \tag{2.10a}$$

$$\mathrm{div}\boldsymbol{u} = 0, \tag{2.10b}$$

$$\frac{\partial c_i}{\partial t} + \nabla\cdot(c_i\boldsymbol{v}_i) = 0, \qquad i = 1, 2, \cdots, m, \tag{2.10c}$$

$$-\hat{\alpha}\nabla c_i + \hat{\beta}c_i z_i \boldsymbol{E} + \hat{\beta}\epsilon c_i z_i \boldsymbol{v}_i \times \boldsymbol{B} = f_{r,i}c_i(\boldsymbol{v}_i - \boldsymbol{u}), \qquad i = 1, 2, \cdots, m, \tag{2.10d}$$

$$\nabla\times\boldsymbol{E} + \epsilon\frac{\partial \boldsymbol{B}}{\partial t} = \boldsymbol{0}, \tag{2.10e}$$

$$\nabla\times\boldsymbol{B} - \epsilon\frac{\partial \boldsymbol{E}}{\partial t} = \epsilon R\sum_{i=1}^{m} c_i z_i \boldsymbol{v}_i, \tag{2.10f}$$

where $R_e = \rho L u_0/\eta$ is the Reynolds number, $f_{r,i} = \xi_i c_0 L/(\rho u_0)$ is a friction coefficient, $\hat{\alpha} = \alpha c_0/(\rho u_0^2)$, $\hat{\beta} = z_0 c_0 E_0 L/\left(\rho u_0^2\right)$, $\epsilon = u_0/\mathrm{c}$ and $R = c_0 z_0 L/(E_0\varepsilon_0)$.

Since the velocity of the fluid is small compared to the speed of light, the Lorentz force term $\hat{\beta}\epsilon c_i z_i \boldsymbol{v}_i \times \boldsymbol{B}$ is small relative to the other terms in (2.10d). Then we ignore this term in (2.10d) and derive a relation

$$f_{r,i}c_i(\boldsymbol{v}_i - \boldsymbol{u}) = -\hat{\alpha}\nabla c_i + \hat{\beta}c_i z_i \boldsymbol{E}, \quad i = 1, 2, \cdots, m. \tag{2.11}$$

We substitute the relation to other equations in (2.10) to eliminate $\boldsymbol{v}_i$. This leads to

$$\frac{\partial \boldsymbol{u}}{\partial t} + \boldsymbol{u}\cdot\nabla\boldsymbol{u} - R_e^{-1}\Delta\boldsymbol{u} + \nabla p + \sum_{i=1}^{m}\hat{\alpha}\nabla c_i = \sum_{i=1}^{m}\hat{\beta}c_i z_i \boldsymbol{E}, \tag{2.12a}$$

$$\mathrm{div}\boldsymbol{u} = 0, \tag{2.12b}$$

$$\frac{\partial c_i}{\partial t} + \nabla\cdot(c_i\boldsymbol{u}) - D_i\Delta c_i + \beta_i\nabla\cdot(c_i z_i \boldsymbol{E}) = 0, \quad i = 1, 2, \cdots, m, \tag{2.12c}$$

$$\nabla\times\boldsymbol{E} + \epsilon\frac{\partial \boldsymbol{B}}{\partial t} = \boldsymbol{0}, \tag{2.12d}$$

$$\nabla\times\boldsymbol{B} - \epsilon\frac{\partial \boldsymbol{E}}{\partial t} = \epsilon R\sum_{i=1}^{m}\left(c_i z_i \boldsymbol{u} - z_i D_i\nabla c_i + \beta_i c_i z_i^2 \boldsymbol{E}\right), \tag{2.12e}$$

where $D_i = \hat{\alpha}/f_{r,i}$ is the (dimensionless) diffusion coefficient and $\beta_i = \hat{\beta}/f_{r,i}$ is the drift coefficient. To close the system, we set the initial and boundary conditions as

$$\boldsymbol{u}(x,0) = \boldsymbol{u}^0, \quad c_i(x,0) = c_i^0, \quad \boldsymbol{B}(x,0) = \boldsymbol{B}^0, \quad \boldsymbol{E}(x,0) = \boldsymbol{E}^0 \quad \text{in} \quad \Omega, \tag{2.13}$$

$$\boldsymbol{u} = \boldsymbol{0}, \quad (-D_i\nabla c_i + c_i\boldsymbol{u} + \beta_i c_i z_i \boldsymbol{E})\cdot\boldsymbol{n} = 0, \quad \boldsymbol{B}\times\boldsymbol{n} = \boldsymbol{0} \quad \text{on} \quad \Gamma, \tag{2.14}$$

where $\boldsymbol{u}^0$ and $\boldsymbol{B}^0$ satisfy $\nabla\cdot\boldsymbol{u}^0=\nabla\cdot\boldsymbol{B}^0=0$. We would like to address that the boundary condition for the magnetic field $\boldsymbol{B}$ also implies a boundary condition for the electric field $\boldsymbol{E}$,

$$\boldsymbol{E}\cdot\boldsymbol{n}=0 \quad \text{on} \quad \Gamma. \tag{2.15}$$

Actually, by using (2.12e), (2.14) and the fact that $\mathrm{div}_\Gamma(\boldsymbol{B}\times\boldsymbol{n})=\mathbf{curl}\times\boldsymbol{B}\cdot\boldsymbol{n}$ [34], we deduce $\partial(\boldsymbol{E}\cdot\boldsymbol{n})/\partial t=0$ on Γ. Thus, (2.15) follows provided that the initial electric field satisfies $\boldsymbol{E}^0\cdot\boldsymbol{n}=0$ on Γ.

2.3. Some key properties. We first prove the non-negativity of the ion concentrations of the NSNPM model in the following proposition.

PROPOSITION 2.1 (Non-negativity). *If the initial ion concentrations are non-negative,*

$$c_i^0(x,0)\geq 0, \quad i=1,2,\cdots,m, \quad \text{a.e. } x\in\Omega,$$

then the ion concentrations of the NSNPM model (2.12) *are non-negative, that is*

$$c_i(x,t)\geq 0, \quad i=1,2,\cdots,m, \quad \text{a.e. } x\in\Omega, \quad \forall t>0. \tag{2.16}$$

Proof. Following [40, 16], we first introduce the auxiliary problem,

$$\frac{\partial c_i}{\partial t}+\nabla\cdot(c_i^+\boldsymbol{u})-D_i\Delta c_i+\beta_i\nabla\cdot(c_i^+z_i\boldsymbol{E})=0, \tag{2.17}$$

where $c_i^+\coloneqq\sup\{c_i,0\}$. Obviously, if c_i is the solution to (2.12c) and satisfies $c_i\geq 0$, then it is the solution to (2.17). Conversely, if c_i is the solution to (2.17) and satisfies $c_i\geq 0$, then it is also the solution to (2.12c).

Define $c_i^-\coloneqq\sup\{-c_i,0\}$, we can write c_i as $c_i=c_i^+-c_i^-$. Multiplying (2.17) by c_i^- and integrating by parts, we have

$$\frac{1}{2}\frac{\mathrm{d}}{\mathrm{d}t}\left\|c_i^-\right\|^2+D_i\left\|\nabla c_i^-\right\|^2=\int_\Omega c_i^+(\boldsymbol{u}+\beta_i z_i\boldsymbol{E})\cdot\nabla c_i^-=0,$$

where we have used the properties of c_i^- and ∇c_i^-, the boundary conditions (2.14) and (2.15), see [18]. Then, we integrate the above equation over $(0,t)$ and use the non-negativity of the initial ion concentrations to deduce

$$\|c_i^-(x,t)\|^2=\|(c_i^0)^-\|^2-\int_0^t\|\nabla c_i^-(x,s)\|^2\mathrm{d}s=-\int_0^t\|\nabla c_i^-(x,s)\|^2\mathrm{d}s\leq 0.$$

This yields $c_i^-(x,t)=0$, so that the solution of the auxiliary problem (2.17) satisfies $c_i(x,t)\geq 0$. Therefore, c_i is also a solution of the original problem (2.12c) and non-negative. The proof is complete. ∎

Then, we can easily prove the mass conservation for each type of ions in the solution, as shown in the following proposition.

PROPOSITION 2.2 (Mass conservation). *The mass of the model is conservated in the following sense,*

$$\int_\Omega c_i(x,t)=\int_\Omega c_i(x,0), \quad \forall t>0. \tag{2.18}$$

Proof. Integrating (2.12c) over Ω, using the integration by parts and (2.14), we obtain (2.18). ∎

Next, we present the magnetic-flux conservation for the magnetic field in the solution in the following proposition. This property is a precise physical law in electromagnetics, which means that there is no source of the magnetic field in the domain.

PROPOSITION 2.3 (Magnetic-flux conservation). *The magnetic flux of the model is conservated in the following sense,*

$$\nabla\cdot\boldsymbol{B}=0, \quad \forall t>0. \tag{2.19}$$

In the following theorem, we present an energy dissipation property for the system (2.12). Hereinafter, we assume that $c_i(\boldsymbol{x},t)\neq 0$ in Ω.

THEOREM 2.1 (Energy dissipation). *The NSNPM equations (2.12)-(2.14) satisfy the energy dissipation relation,*

$$\frac{\mathrm{d}\mathcal{E}}{\mathrm{d}t}=-\mathcal{R}, \tag{2.20}$$

where the energy and the dissipation terms are respectively given by

$$\mathcal{E}=\int_\Omega \frac{1}{2}|\boldsymbol{u}|^2+\sum_{i=1}^m\int_\Omega \hat{\alpha}c_i\log c_i+\int_\Omega \frac{\hat{\beta}}{R}\left(\frac{1}{2}|\boldsymbol{B}|^2+\frac{1}{2}|\boldsymbol{E}|^2\right),$$
$$\mathcal{R}=R_e^{-1}\int_\Omega |\nabla\boldsymbol{u}|^2+\sum_{i=1}^m\int_\Omega c_i\left|\frac{\sqrt{\hat{\alpha}D_i}}{c_i}\nabla c_i-\sqrt{\hat{\beta}\beta_i}z_i\boldsymbol{E}\right|^2.$$

Proof. By taking the $\boldsymbol{L}^2$-inner product of (2.12a) with $\boldsymbol{u}$, using the integration by parts, $(\boldsymbol{u}\cdot\nabla\boldsymbol{u},\boldsymbol{u})=0$, and (2.12b), we get

$$\frac{\mathrm{d}}{\mathrm{d}t}\int_\Omega\frac{1}{2}|\boldsymbol{u}|^2+R_e^{-1}\int_\Omega|\nabla\boldsymbol{u}|^2+\sum_{i=1}^m\int_\Omega\hat{\alpha}\nabla c_i\cdot\boldsymbol{u}=\sum_{i=1}^m\int_\Omega\hat{\beta}c_iz_i\boldsymbol{E}\cdot\boldsymbol{u}. \tag{2.21}$$

By taking the $\boldsymbol{L}^2$-inner product of (2.12c) with $\log c_i+1$, integrating by parts and using (2.14), $\nabla c_i=c_i\nabla(\log c_i)$ and (2.12b), we have for $i=1,2,\cdots,m$,

$$\frac{\mathrm{d}}{\mathrm{d}t}\int_\Omega c_i\log c_i+D_i\int_\Omega c_i\left|\frac{1}{c_i}\nabla c_i\right|^2=\int_\Omega\boldsymbol{u}\cdot\nabla c_i+\int_\Omega\beta_iz_i\boldsymbol{E}\cdot\nabla c_i. \tag{2.22}$$

Multiplying $\hat{\alpha}$ to the above equation and summing them up for $i=1,2,\cdots,m$, we get

$$\frac{\mathrm{d}}{\mathrm{d}t}\sum_{i=1}^m\int_\Omega\hat{\alpha}c_i\log c_i+\sum_{i=1}^m\hat{\alpha}D_i\int_\Omega c_i\left|\frac{1}{c_i}\nabla c_i\right|^2=\sum_{i=1}^m\int_\Omega\hat{\alpha}\boldsymbol{u}\cdot\nabla c_i+\sum_{i=1}^m\int_\Omega\hat{\alpha}\beta_iz_i\boldsymbol{E}\cdot\nabla c_i. \tag{2.23}$$

By taking the $\boldsymbol{L}^2$-inner product of (2.12d) with $\boldsymbol{B}$, we have

$$\int_\Omega\nabla\times\boldsymbol{E}\cdot\boldsymbol{B}+\frac{\mathrm{d}}{\mathrm{d}t}\int_\Omega\frac{\epsilon}{2}|\boldsymbol{B}|^2=0.$$

By taking the $\boldsymbol{L}^2$-inner product of (2.12e) with $\boldsymbol{E}$, using the integration by parts and (2.14), we get

$$\int_\Omega\boldsymbol{B}\cdot\nabla\times\boldsymbol{E}-\frac{\mathrm{d}}{\mathrm{d}t}\int_\Omega\frac{\epsilon}{2}|\boldsymbol{E}|^2=\sum_{i=1}^n\int_\Omega\epsilon R\left(c_iz_i\boldsymbol{u}-z_iD_i\nabla c_i+\beta_ic_iz_i^2\boldsymbol{E}\right)\cdot\boldsymbol{E}.$$

Multiplying $\hat{\beta}/(\epsilon R)$ to the above two equations and summing them up, we obtain

$$\frac{\mathrm{d}}{\mathrm{d}t}\int_\Omega\frac{\hat{\beta}}{R}\left(\frac{1}{2}|\boldsymbol{B}|^2+\frac{1}{2}|\boldsymbol{E}|^2\right)=-\sum_{i=1}^m\int_\Omega\hat{\beta}\left(c_iz_i\boldsymbol{u}-z_iD_i\nabla c_i+\beta_ic_iz_i^2\boldsymbol{E}\right)\cdot\boldsymbol{E}. \tag{2.24}$$

Then, combining (2.21)-(2.24) and using the relation that $\hat{\alpha}\beta_i=\hat{\beta}D_i$, we have

$$\begin{aligned}
&\frac{\mathrm{d}}{\mathrm{d}t}\int_\Omega \frac{1}{2}|\boldsymbol{u}|^2 + \frac{\mathrm{d}}{\mathrm{d}t}\sum_{i=1}^m \int_\Omega \hat{\alpha} c_i \log c_i + \frac{\mathrm{d}}{\mathrm{d}t}\int_\Omega \frac{\hat{\beta}}{R}\left(\frac{1}{2}|\boldsymbol{B}|^2 + \frac{1}{2}|\boldsymbol{E}|^2\right)\\
&= -R_e^{-1}\int_\Omega |\nabla \boldsymbol{u}|^2 - \sum_{i=1}^m \hat{\alpha} D_i \int_\Omega c_i \left|\frac{1}{c_i}\nabla c_i\right|^2 + \sum_{i=1}^m \int_\Omega \hat{\alpha}\beta_i z_i \boldsymbol{E}\cdot\nabla c_i + \sum_{i=1}^n \int_\Omega \hat{\beta}\left(z_i D_i \nabla c_i - \beta_i c_i z_i^2 \boldsymbol{E}\right)\cdot \boldsymbol{E}\\
&= -R_e^{-1}\int_\Omega |\nabla \boldsymbol{u}|^2 - \sum_{i=1}^m \int_\Omega c_i \left|\frac{\sqrt{\hat{\alpha} D_i}}{c_i}\nabla c_i - \sqrt{\hat{\beta}\beta_i} z_i \boldsymbol{E}\right|^2.
\end{aligned}$$

The proof is complete. ∎

REMARK 2.1. *The last term in the dissipation function $\mathcal{R}$ looks very complicated. But it has clear physical meanings as shown below. Notice that*

$$\frac{\sqrt{\hat{\alpha} D_i}}{c_i}\nabla c_i - \sqrt{\hat{\beta}\beta_i} z_i \boldsymbol{E} = \frac{1}{\sqrt{f_{r,i}}}\left(\frac{\hat{\alpha}}{c_i}\nabla c_i - \hat{\beta} z_i \boldsymbol{E}\right) = -\sqrt{f_{r,i}}(\boldsymbol{v}_i - \boldsymbol{u}),$$

where we have used (2.11) in the last equation. Then the last term of $\mathcal{R}$ is reduced to $\int_\Omega f_{r,i} c_i |\boldsymbol{v}_i - \boldsymbol{u}|^2 \mathrm{d}x$. This is the energy dissipation due to the friction between the ion molecular and the solution.

REMARK 2.2. *Notice that the gradient term $\sum_{i=1}^m \hat{\alpha}\nabla c_i$ in (2.12a) can be absorbed into the pressure term by setting $\tilde{p} = p + \sum_{i=1}^m \hat{\alpha} c_i$, as in the standard Naver-Stokes-Possion-Nernst-Planck system [40]. However, we would like to remark that it will be convenient for us to design stable and efficient numerical schemes when keeping the gradient term as in (2.12a). We will give some explanation below. It is known that the proof of the discrete energy law for a numerical scheme usually follows the same line as for the continuous system. From (2.21) and (2.23), we can see that the coupling terms $\sum_{i=1}^m \int_\Omega \hat{\alpha}\nabla c_i \cdot \boldsymbol{u}$ cancel each other out directly. However, once we absorb the gradient term into the pressure, the term $\hat{\alpha}\int_\Omega \boldsymbol{u}\cdot\nabla c_i$ in the concentration equation (2.23) can not be canceled and we have to do integrate by parts and use (2.12b), to derive $\int_\Omega \boldsymbol{u}\cdot\nabla c_i = -\int_\Omega \nabla\cdot\boldsymbol{u} c_i = 0$. By doing so, we can prove that the energy dissipation property still holds on the continuous level. However, if we generalize the proof to the discrete case, we need to make sure the discrete velocity satisfies the same divergence-free property. This is not an easy task for standard numerical methods. That is why a $\boldsymbol{H}(\mathrm{div})$-based discontinuous Galerkin methods [7] and a virtual finite element method [13] have been proposed for the Naver-Stokes-Possion-Nernst-Planck system in literature. Our strategy to keep the term $\sum_{i=1}^m \hat{\alpha}\nabla c_i$ in (2.12a) can essentially overcome the difficulty, which makes many commonly used finite element pairs preserve the energy dissipation law, as shown in the Section 4. The technique applies also to the standard Naver-Stokes-Possion-Nernst-Planck system.*

2.4. The log-density formulation. The NSNPM system (2.12) is a highly nonlinear, coupled multiphysics PDE system, making it challenging to solve numerically. Furthermore, designing numerical methods that preserve the physical properties discussed in the previous subsection adds to the complexity. To ensure that the ion densities c_i remain positive, we implement the following transformation (as in [33, 7])

$$\eta_i = \log c_i \quad \text{so that } \nabla c_i = e^{\eta_i}\nabla\eta_i.$$

We will use η_i as unknowns instead of c_i. The transformed system is given by

$$\frac{\partial \boldsymbol{u}}{\partial t} + \boldsymbol{u}\cdot\nabla\boldsymbol{u} - R_e^{-1}\Delta\boldsymbol{u} + \nabla p + \sum_{i=1}^m \hat{\alpha} e^{\eta_i}\nabla\eta_i = \sum_{i=1}^m \hat{\beta} e^{\eta_i} z_i \boldsymbol{E}, \tag{2.25a}$$

$$\mathrm{div}\boldsymbol{u} = 0, \tag{2.25b}$$

$$\frac{\partial e^{\eta_i}}{\partial t} + \nabla\cdot(e^{\eta_i}\boldsymbol{u}) - D_i\nabla\cdot(e^{\eta_i}\nabla\eta_i) + \beta_i\nabla\cdot(e^{\eta_i} z_i \boldsymbol{E}) = 0, \quad i = 1, 2, \cdots, m, \tag{2.25c}$$

$$\nabla \times \boldsymbol{E} + \epsilon \frac{\partial \boldsymbol{B}}{\partial t} = \boldsymbol{0}, \tag{2.25d}$$

$$\nabla \times \boldsymbol{B} - \epsilon \frac{\partial \boldsymbol{E}}{\partial t} = \epsilon R \sum_{i=1}^{m} \left(e^{\eta_i} z_i \boldsymbol{u} - z_i D_i e^{\eta_i} \nabla \eta_i + \beta_i e^{\eta_i} z_i^2 \boldsymbol{E} \right). \tag{2.25e}$$

The initial and boundary conditions are correspondingly changed to

$$\boldsymbol{u}(0) = \boldsymbol{u}^0, \quad \eta_i(0) = \eta_i^0, \quad \boldsymbol{B}(0) = \boldsymbol{B}^0, \quad \boldsymbol{E}(0) = \boldsymbol{E}^0 \quad \text{in } \Omega, \tag{2.26}$$

$$\boldsymbol{u} = \boldsymbol{0}, \quad (-D_i \nabla \eta_i + \boldsymbol{u} + \beta_i z_i \boldsymbol{E}) \cdot \boldsymbol{n} = 0, \quad \boldsymbol{B} \times \boldsymbol{n} = \boldsymbol{0} \quad \text{on } \Gamma. \tag{2.27}$$

3. Numerical Methods. In this section, we first introduce the weak form for the system (2.25). Then we introduce a fully decoupled method for the system.

3.1. The weak form. We start by introducing some notations. As usual, the inner product and norm in $L^2(\Omega)$ are denoted by $(\cdot,\cdot)$ and $\|\cdot\|$, respectively. For convenience in later use, we introduce some function spaces

$$\begin{aligned} S &:= H^1(\Omega), \ Q := L_0^2(\Omega) = \left\{ q \in L^2(\Omega), (q,1) = 0 \right\}, \\ \boldsymbol{V} &:= \boldsymbol{H}_0^1(\Omega) = \left\{ \boldsymbol{v} \in \boldsymbol{H}^1(\Omega), \boldsymbol{v}|_\Gamma = 0 \right\}, \\ \boldsymbol{W} &:= \boldsymbol{H}(\mathbf{curl}, \Omega) = \left\{ \boldsymbol{M} \in \boldsymbol{L}^2(\Omega), \nabla \times \boldsymbol{M} \in \boldsymbol{L}^2(\Omega) \right\}, \\ \boldsymbol{D} &:= \boldsymbol{H}(\mathrm{div}, \Omega) = \left\{ \boldsymbol{C} \in \boldsymbol{L}^2(\Omega), \nabla \cdot \boldsymbol{C} \in L^2(\Omega) \right\}. \end{aligned}$$

The standard norms in $\boldsymbol{H}(\mathrm{div}, \Omega)$ and $\boldsymbol{H}(\mathbf{curl}, \Omega)$ are denoted by $\|\cdot\|_{\mathrm{div}}$ and $\|\cdot\|_{\mathbf{curl}}$, respectively. In order to deal with the convection term in (2.25a), we define the following trilinear form for $\boldsymbol{u}, \boldsymbol{v}, \boldsymbol{w} \in \boldsymbol{V}$,

$$\mathcal{O}(\boldsymbol{u}, \boldsymbol{v}, \boldsymbol{w}) := \frac{1}{2} \left((\boldsymbol{u} \cdot \nabla \boldsymbol{v}, \boldsymbol{w}) - (\boldsymbol{u} \cdot \nabla \boldsymbol{w}, \boldsymbol{v}) \right)$$

Then we can derive the weak form of the NSNPM system (2.25) by standard approach. It is to find $(\boldsymbol{u}, p, \boldsymbol{B}, \boldsymbol{E}) \in \boldsymbol{V} \times Q \times \boldsymbol{W} \times \boldsymbol{D}$ and $\eta_i \in S$, $i = 1, 2, \cdots, m$, such that the following equations hold

$$(\partial_t \boldsymbol{u}, \boldsymbol{v}) + R_e^{-1} (\nabla \boldsymbol{u}, \nabla \boldsymbol{v}) + \mathcal{O}(\boldsymbol{u}, \boldsymbol{u}, \boldsymbol{v}) - (p, \nabla \cdot \boldsymbol{v}) + \sum_{i=1}^{m} (\hat{\alpha} e^{\eta_i} \nabla \eta_i, \boldsymbol{v}) - \sum_{i=1}^{m} \left(\hat{\beta} e^{\eta_i} z_i \boldsymbol{E}, \boldsymbol{v} \right) = 0, \tag{3.1a}$$

$$(\nabla \cdot \boldsymbol{u}, q) = 0, \tag{3.1b}$$

$$(\partial_t e^{\eta_i}, s) - (\boldsymbol{u} e^{\eta_i}, \nabla s) + (D_i e^{\eta_i} \nabla \eta_i, \nabla s) - (\beta_i e^{\eta_i} z_i \boldsymbol{E}, \nabla s) = 0, \quad i = 1, 2, \cdots, m, \tag{3.1c}$$

$$(\epsilon \partial_t \boldsymbol{B}, \boldsymbol{C}) + (\nabla \times \boldsymbol{E}, \boldsymbol{C}) = 0, \tag{3.1d}$$

$$(\boldsymbol{B}, \nabla \times \boldsymbol{M}) - (\epsilon \partial_t \boldsymbol{E}, \boldsymbol{M}) - \sum_{i=1}^{m} \left(\epsilon R \left(e^{\eta_i} z_i \boldsymbol{u} - z_i D_i e^{\eta_i} \nabla \eta_i + \beta_i e^{\eta_i} z_i^2 \boldsymbol{E} \right), \boldsymbol{M} \right) = 0, \tag{3.1e}$$

for all $(\boldsymbol{v}, q, \boldsymbol{C}, \boldsymbol{M}) \in \boldsymbol{V} \times Q \times \boldsymbol{W} \times \boldsymbol{D}$ and $s \in S$. In the following, we will consider the space and time discretization to the weak problem.

3.2. A decoupled numerical scheme. For the time discretization, let $\{t_n = n\tau : \ n = 0, 1, \cdots, N\}$, $\tau = T/N$, be an equidistant partition of $[0, T]$. Given a function $v(x,t)$, the semidiscrete approximation to $v(x, t_n)$ will be denoted by $v^n(x)$. For $n \geq 1$ and any function v, we define the first-order backward finite difference operator as $\delta_t v^n = (v^n - v^{n-1})/\tau$.

For the space discretization, let $\mathcal{T}_h$ be a quasi-uniform and shape-regular tetrahedral mesh of Ω. Denote the local mesh size by $h_K = \mathrm{diam}(K)$ and the global mesh size by $h := \max_{K \in \mathcal{T}_h} h_K$. For any integer $k \geq 0$, let $P_k(K)$ be the space of polynomials of degree k on element K and define $\boldsymbol{P}_k(K) = P_k(K)^3$. To approximate

the unknown functions η_i, we adopt a conforming finite element space $S_h \subset S$. To approximate the velocity and pressure $(\boldsymbol{u}, p)$, we use a conforming finite element pair $(\boldsymbol{V}_h \times Q_h) \subset (\boldsymbol{V} \times Q)$, which satisfies the discrete inf-sup condition,

$$\inf_{0\neq q_h\in Q_h}\sup_{\boldsymbol{0}\neq \boldsymbol{v}_h\in \boldsymbol{V}_h}\frac{(q_h,\mathrm{div}\boldsymbol{v}_h)}{\|\nabla \boldsymbol{v}_h\|\,\|q_h\|}\geq \beta_s, \tag{3.2}$$

where β_s is a positive constant independent of mesh size h. To approximate the magnetic field $\boldsymbol{B}$, we employ a conforming finite element space $\boldsymbol{D}_h \subset \boldsymbol{D}$. To approximate the electric field $\boldsymbol{E}$, we utilize a conforming finite element space $\boldsymbol{W}_h \subset \boldsymbol{W}$. In addition, the electromagnetic pair $(\boldsymbol{W}_h, \boldsymbol{D}_h)$ should meet the following de-Rham sequence,

$$\begin{array}{ccccccc} H^1(\Omega) & \xrightarrow{\text{grad}} & \boldsymbol{W} & \xrightarrow{\text{curl}} & \boldsymbol{D} & \xrightarrow{\text{div}} & L^2(\Omega) \\ \downarrow \Pi_h^{\text{grad}} & & \downarrow \Pi_h^{\text{curl}} & & \downarrow \Pi_h^{\text{div}} & & \downarrow \Pi_h^0, \\ V_h & \xrightarrow{\text{grad}} & \boldsymbol{W}_h & \xrightarrow{\text{curl}} & \boldsymbol{D}_h & \xrightarrow{\text{div}} & R_h \end{array} \tag{3.3}$$

where $V_h \subset H^1(\Omega)$ and $R_h \subset L^2(\Omega)$ are conforming finite element spaces, Π_h^{grad}, Π_h^{curl}, Π_h^{div} and Π_h^0 are the corresponding standard interpolation operators. We will utilize the lowest-order finite element spaces in our numerical experiments in Section 5. The theoretical analysis presented in this section and the next is applicable to various other pairs of stable finite element pairs (see [19, 6, 26]). For convenience, we write the standard interpolation operators of $\boldsymbol{V}_h$ and S_h as $\Pi_{0,h}^{\text{grad}}$ and $\Pi_{1,h}^{\text{grad}}$, respectively.

Inspired by the stabilization method in [41, 42], we propose a decoupled first-order scheme for solving the system (2.12). At the initial time step, we set $\boldsymbol{u}_h^0 = \boldsymbol{\Pi}_{0,h}^{\text{grad}}\boldsymbol{u}^0$, $\eta_{i,h}^0 = \Pi_{1,h}^{\text{grad}}\eta_i^0$, $i = 1, 2, \cdots, m$, $\boldsymbol{B}_h^0 = \Pi_h^{\text{div}}\boldsymbol{B}^0$ and $\boldsymbol{E}_h^0 = \Pi_h^{\text{curl}}\boldsymbol{E}^0$. For $n \geq 1$, we compute $\left(\boldsymbol{u}_h^{n+1}, p_h^{n+1}, \boldsymbol{B}_h^{n+1}, \boldsymbol{E}_h^{n+1}\right) \in \boldsymbol{V}_h \times Q_h \times \boldsymbol{D}_h \times \boldsymbol{W}_h$ and $\eta_{i,h}^{n+1} \in S_h$, $i = 1, 2, \cdots, m$, by solving the following three substeps:

Step 1: Find $\eta_{i,h}^{n+1} \in S_h$, $i = 1, 2, \cdots, m$, by solving the discrete Nernst-Planck equations separately,

$$(\delta_t e^{\eta_{i,h}^{n+1}}, s_h) - \left(\boldsymbol{u}_h^n e^{\eta_{i,h}^n}, \nabla s_h\right) + \left(D_i e^{\eta_{i,h}^n}\nabla\eta_{i,h}^{n+1}, \nabla s_h\right) - \left(\beta_i e^{\eta_{i,h}^n} z_i \boldsymbol{E}_h^n, \nabla s_h\right) + a_{\text{stab}}^1\left(\eta_{i,h}^{n+1}, s_h\right) = 0, \tag{3.4}$$

for all $s_h \in S_h$, where $a_{\text{stab}}^1(\cdot,\cdot)$ is a bilinear form on $S_h \times S_h$ including two extra first-order stabilization terms,

$$a_{\text{stab}}^1\left(w_h, s_h\right) \coloneqq \tau m\left(\hat{\alpha} e^{\eta_{i,h}^n}\nabla w_h, e^{\eta_{i,h}^n}\nabla s_h\right) + \frac{\tau m}{2}\left(\beta_i z_i^2 D_i R e^{\eta_{i,h}^n}\nabla w_h, e^{\eta_{i,h}^n}\nabla s_h\right). \tag{3.5}$$

Step 2: Find $\left(\boldsymbol{B}_h^{n+1}, \boldsymbol{E}_h^{n+1}\right) \in \boldsymbol{D}_h \times \boldsymbol{W}_h$ by solving the discrete Maxwell equations,

$$\left(\epsilon\delta_t \boldsymbol{B}_h^{n+1}, \boldsymbol{C}_h\right) + \left(\nabla \times \boldsymbol{E}_h^{n+1}, \boldsymbol{C}_h\right) = 0, \tag{3.6a}$$

$$\begin{aligned}\left(\boldsymbol{B}_h^{n+1}, \nabla\times\boldsymbol{M}_h\right) - \left(\epsilon\delta_t \boldsymbol{E}_h^{n+1}, \boldsymbol{M}_h\right) - \sum_{i=1}^m\left(\epsilon R\left(e^{\eta_{i,h}^n} z_i \boldsymbol{u}_h^n - z_i D_i e^{\eta_{i,h}^n}\nabla\eta_{i,h}^{n+1}\right), \boldsymbol{M}_h\right) \\ - \sum_{i=1}^m\left(\epsilon R\beta_i e^{\eta_{i,h}^n} z_i^2 \boldsymbol{E}_h^{n+1}, \boldsymbol{M}_h\right) - a_{\text{stab}}^2\left(\boldsymbol{E}_h^{n+1}, \boldsymbol{M}_h\right) = 0,\end{aligned} \tag{3.6b}$$

for all $(\boldsymbol{C}_h, \boldsymbol{M}_h) \in \boldsymbol{D}_h \times \boldsymbol{W}_h$, where $a_{\text{stab}}^2(\cdot,\cdot)$ is a bilinear form on $\boldsymbol{W}_h \times \boldsymbol{W}_h$ including one extra first-order stabilization term,

$$a_{\text{stab}}^2(\boldsymbol{N}_h, \boldsymbol{M}_h) \coloneqq \tau\left(\epsilon R\hat{\beta}\sum_{i=1}^m e^{\eta_{i,h}^n} z_i \sum_{j=1}^m e^{\eta_{j,h}^n} z_j \boldsymbol{N}_h, \boldsymbol{M}_h\right). \tag{3.7}$$

Step 3: Find $\left(\boldsymbol{u}_h^{n+1}, p_h^{n+1}\right) \in \boldsymbol{V}_h \times Q_h$ by solving the discrete Navier-Stokes equations,

$$\begin{aligned}\left(\delta_t \boldsymbol{u}_h^{n+1}, \boldsymbol{v}_h\right) + R_e^{-1}\left(\nabla \boldsymbol{u}_h^{n+1}, \nabla \boldsymbol{v}_h\right) + \gamma(\nabla \cdot \boldsymbol{u}_h^{n+1}, \nabla \cdot \boldsymbol{v}_h) + \mathcal{O}\left(\boldsymbol{u}_h^n, \boldsymbol{u}_h^{n+1}, \boldsymbol{v}_h\right) \\ - \left(p_h^{n+1}, \nabla \cdot \boldsymbol{v}_h\right) + \sum_{i=1}^{m}\left(\hat{\alpha} e^{\eta_{i,h}^n} \nabla \eta_{i,h}^{n+1}, \boldsymbol{v}_h\right) - \sum_{i=1}^{m}\left(\hat{\beta} e^{\eta_{i,h}^n} z_i \boldsymbol{E}_h^{n+1}, \boldsymbol{v}_h\right) = 0, \qquad (3.8a)\end{aligned}$$

$$\left(\nabla \cdot \boldsymbol{u}_h^{n+1}, q_h\right) = 0, \qquad (3.8b)$$

for all $(\boldsymbol{v}_h, q_h) \in \boldsymbol{V}_h \times Q_h$, where $\gamma > 0$ is the stabilization parameter.

REMARK 3.1. *We explain the strategy behind developing the above scheme.*

*(i) In **Step 1** of (3.4), we add two first-order stabilized terms (3.5) to balance the explicit treatment of the velocity and electric field in the coupling terms. These perturbation terms are important in decoupling the computation of Nernst-Planck equations from the Navier-Stokes equations and Maxwell equations while ensuring the unconditional energy stability. Particularly, we can compute the ion concentration η_i separately for each i. The details can be found in the proof of Theorem 4.1.*

*(ii) In **Step 2** of (3.6b), we also introduce a stabilized term (3.7) to balance the explicit treatment of the velocity in the coupling term. This term is important in decoupling the computation of the Maxwell equations from the Navier-Stokes equations while ensuring the unconditional energy stability.*

*(iii) In **Step 3**, we introduce an augmented Lagrangian stabilization to control the divergence of discrete velocity and relax the effects of the pressure error on the velocity error in (3.8a). In addition, this stabilization has advantages in designing robust solvers for the discrete problems, especially when the Reynolds number is large [30, 11]. Without further specification, we choose $\gamma = 1$ in our numerical tests.*

Thanks to the structure-preserving property of finite element pair $(\boldsymbol{W}_h, \boldsymbol{D}_h)$, we can further decouple the computations of the magnetic field and electric field. Specifically, invoking with (3.3), we notice that $\nabla \times \boldsymbol{W}_h \subset \boldsymbol{D}_h$. Thus, for any $\boldsymbol{M}_h \in \boldsymbol{W}_h$, taking $\boldsymbol{C}_h = \nabla \times \boldsymbol{M}_h$ in (3.6a), we have

$$\left(\epsilon \delta_t \boldsymbol{B}_h^{n+1}, \nabla \times \boldsymbol{M}_h\right) + \left(\nabla \times \boldsymbol{E}_h^{n+1}, \nabla \times \boldsymbol{M}_h\right) = 0. \qquad (3.9)$$

Then we plug (3.9) into (3.6b) to get

$$\begin{aligned}\left(\boldsymbol{B}_h^n, \nabla \times \boldsymbol{M}_h\right) - \tau \epsilon^{-1}\left(\nabla \times \boldsymbol{E}_h^{n+1}, \nabla \times \boldsymbol{M}_h\right) - \left(\epsilon \delta_t \boldsymbol{E}_h^{n+1}, \boldsymbol{M}_h\right) \\ - \left(\epsilon R \sum_{i=1}^{m}\left(e^{\eta_{i,h}^n} z_i \boldsymbol{u}_h^n - z_i D_i e^{\eta_{i,h}^n} \nabla \eta_{i,h}^{n+1} + \beta_i e^{\eta_{i,h}^n} z_i^2 \boldsymbol{E}_h^{n+1}\right), \boldsymbol{M}_h\right) - a_{\text{stab}}^2\left(\boldsymbol{E}_h^{n+1}, \boldsymbol{M}_h\right) = 0. \qquad (3.10)\end{aligned}$$

This is an equation with only one unknown function $\boldsymbol{E}_h^{n+1}$, which can be solved independently. Thus, we can rewrite **Step 2** equivalently into the following two substeps:

Step 2.1 : Find $\boldsymbol{E}_h^{n+1} \in \boldsymbol{W}_h$ such that (3.10) holds for any $\boldsymbol{M}_h \in \boldsymbol{W}_h$.

Step 2.2 : Update $\boldsymbol{B}_h^{n+1} \in \boldsymbol{D}_h$ by

$$\boldsymbol{B}_h^{n+1} = \boldsymbol{B}_h^n - \tau \epsilon^{-1} \nabla \times \boldsymbol{E}_h^{n+1}. \qquad (3.11)$$

In summary, the fully discrete decoupled scheme is stated in detail in Algorithm 1.

Before proceeding with the analysis, we present some additional comments on the decoupled scheme. First, we we want to emphasize that retaining the gradient term $\sum_{i=1}^{m}\left(\hat{\alpha} \nabla e^{\eta_{i,h}^{n+1}}, \boldsymbol{v}_h\right)$ in the Navier-Stokes equation (3.8) eliminates the cumbersome assumption regarding the finite element spaces $(\boldsymbol{V}_h, Q_h)$ that $\nabla \cdot \boldsymbol{V}_h \subset Q_h$ (as discussed in Remark 2.2). This assumption is essential for demonstrating the energy stability properties within the numerical schemes, even for the Navier-Stokes-Poisson-Nernst-Planck system [7, 13]. Second, we initialize the magnetic field as $\boldsymbol{B}_h^0 = \Pi_h^{\text{div}} \boldsymbol{B}^0$ to ensure that $\nabla \cdot \boldsymbol{B}_h^0 = 0$, where Π_h^{div} is the canonical interpolation operator in (3.3). This is justified by the following commutativity: $\nabla \cdot \boldsymbol{B}_h^0 = \nabla \cdot \left(\Pi_h^{\text{div}} \boldsymbol{B}^0\right) =$

Algorithm 1: The fully decoupled numerical scheme

Data: Initial values and boundary values for the system (2.25)
Result: The discrete solution at time $t = T$.
Partition the time interval $(0, T)$, triangulate the space domain Ω and interpolate the initial values;
while $t_n < T$ **do**
  Step 1 : Solve (3.4) to obtain $\eta_{i,h}^{n+1}$ for $i = 1, \cdots, m$;
  Step 2.1 : Solve (3.10) to obtain $\boldsymbol{E}_h^{n+1}$;
  Step 2.2 : Update $\boldsymbol{B}_h^{n+1}$ directly by (3.11) ;
  Step 3 : Solve (3.8) to obtain $\left(\boldsymbol{u}_h^{n+1}, p_h^{n+1}\right)$;
  Step 4 : $n = n + 1$, $t_n = t_n + \tau$;
end

$\Pi_h^0 \left(\nabla \cdot \boldsymbol{B}^0\right) = 0$. Finally, the velocity and pressure remain coupled in the algorithm. However, one could employ the pressure-correction method [41, 21] or the gauge-Uzawa method [45, 14] to facilitate their decoupling. We choose not to decouple the velocity and pressure because efficient solvers for the stationary Navier-Stokes equations have already been developed in literature.

4. Physics preserving properties. In this section, we will prove that the fully discrete decoupled scheme introduced in the previous section preserves key physical properties similar to those of the continuous model. These properties include mass conservation, positivity of density, magnetic flux conservation, and energy stability.

The positivity and the mass conservation for the ion concentrations computed by the fully discrete scheme are given in the following two propositions.

PROPOSITION 4.1 (Positivity). *The positivity of each ion concentration $c_{i,h}$ follows directly from the exponential formulation that*

$$c_{i,h}^{n+1}(x,t) \coloneqq e^{\eta_{i,h}^{n+1}(x,t)} > 0, \quad i = 1, 2, \cdots, m, \quad \forall n \geq 0. \tag{4.1}$$

PROPOSITION 4.2 (Mass conservation). *The mass of the scheme is conserved in the following sense,*

$$\int_\Omega e^{\eta_{i,h}^{n+1}} = \int_\Omega e^{\eta_{i,h}^{0}}, \quad \forall n \geq 0. \tag{4.2}$$

Proof. By taking $s_h = 1$ in (3.4), we get $(\delta_t e^{\eta_{i,h}^{n+1}}, 1) = 0$. By recursion, we obtain immediately (4.2). ∎

In the following proposition, we will prove that the divergence of the discrete magnetic field is zero. This stems from the argument that the Faraday's law still holds exactly on the discrete level and, as a result, the Gauss's law for the magnetic field is automatically satisfied.

PROPOSITION 4.3 (Magnetic-flux conservation). *The magnetic flux of the scheme is conservated in the following sense,*

$$\nabla \cdot \boldsymbol{B}_h^n = 0, \quad n = 1, 2, \cdots, N. \tag{4.3}$$

Proof. Using $\nabla \times \boldsymbol{W}_h \subset \boldsymbol{D}_h$, we can take $\boldsymbol{C}_h = \epsilon \delta_t \boldsymbol{B}_h^{n+1} + \nabla \times \boldsymbol{E}_h^{n+1}$ in (3.1d) to get

$$\epsilon \delta_t \boldsymbol{B}_h^{n+1} + \nabla \times \boldsymbol{E}_h^{n+1} = \boldsymbol{0}. \tag{4.4}$$

By taking the divergence of (4.4), we have $\nabla \cdot \boldsymbol{B}_h^{n+1} = \nabla \cdot \boldsymbol{B}_h^n$. By recursion, this implies (4.3). ∎

The next theorem presents the energy stability for the decoupled numerical scheme.

THEOREM 4.1 (Energy dissipation). *The scheme (3.4)-(3.8) satisfies an discrete energy dissipation relation,*

$$\delta_t \mathcal{E}_h^{n+1} \le -\mathcal{R}_h^{n+1}, \tag{4.5}$$

where

$$\mathcal{E}_h^n = \int_\Omega \frac{1}{2}|\boldsymbol{u}_h^n|^2 + \sum_{i=1}^m \int_\Omega \hat{\alpha} e^{\eta_{i,h}^n} \eta_{i,h}^n + \int_\Omega \frac{\hat{\beta}}{R}\left(\frac{1}{2}|\boldsymbol{B}_h^n|^2 + \frac{1}{2}|\boldsymbol{E}_h^n|^2\right),$$
$$\mathcal{R}_h^n = R_e^{-1}\int_\Omega |\nabla \boldsymbol{u}_h^n|^2 + \gamma \int_\Omega |\nabla\cdot \boldsymbol{u}_h^n|^2 + \sum_{i=1}^m \int_\Omega e^{\eta_{i,h}^{n-1}} \left|\sqrt{\hat{\alpha} D_i}\nabla \eta_{i,h}^n - \sqrt{\hat{\beta}\beta_i} z_i \boldsymbol{E}_h^n\right|^2.$$

Proof. By taking $\boldsymbol{v}_h = \boldsymbol{u}_h^{n+1}$ in (3.8a) and $q_h = p_h^{n+1}$ in (3.8b), we get

$$\frac{\left\|\boldsymbol{u}_h^{n+1}\right\|^2 - \left\|\boldsymbol{u}_h^n\right\|^2 + \left\|\boldsymbol{u}_h^{n+1} - \boldsymbol{u}_h^n\right\|^2}{2\tau} + R_e^{-1}\left\|\nabla \boldsymbol{u}_h^{n+1}\right\|^2 + \gamma\left\|\nabla\cdot \boldsymbol{u}_h^{n+1}\right\|^2 + \sum_{i=1}^m \left(\hat{\alpha} e^{\eta_{i,h}^n}\nabla \eta_{i,h}^{n+1}, \boldsymbol{u}_h^{n+1}\right)$$
$$= \sum_{i=1}^m \left(\hat{\beta} e^{\eta_{i,h}^n} z_i \boldsymbol{E}_h^{n+1}, \boldsymbol{u}_h^{n+1}\right). \tag{4.6}$$

By taking $s_h = \eta_{i,h}^{n+1} + 1$ in (3.4), we have for $i = 1, 2, \cdots, m$,

$$\left(\delta_t e^{\eta_{i,h}^{n+1}}, \eta_{i,h}^{n+1} + 1\right) + D_i \int_\Omega e^{\eta_{i,h}^n}\left|\nabla \eta_{i,h}^{n+1}\right|^2 + \tau m\hat{\alpha}\int_\Omega \left|e^{\eta_{i,h}^n}\nabla \eta_{i,h}^{n+1}\right|^2 + \frac{\tau m}{2}\beta_i z_i^2 D_i R\int_\Omega \left|e^{\eta_{i,h}^n}\nabla \eta_{i,h}^{n+1}\right|^2$$
$$= \left(\boldsymbol{u}_h^n, e^{\eta_{i,h}^n}\nabla \eta_{i,h}^{n+1}\right) + \left(\beta_i z_i \boldsymbol{E}_h^{n+1}, e^{\eta_{i,h}^n}\nabla \eta_{i,h}^{n+1}\right).$$

To bound the first term on the left-hand side, we use the convexity of the function $f(x) = x(\log x - 1)$ for $x > 0$ to show that

$$(x - y)\log x \ge x(\log x - 1) - y(\log y - 1).$$

This follows from $f'(x) = \log x$, $f''(x) = 1/x > 0$, and Taylor expansion. Applying this bound with $x = e^{\eta_{i,h}^{n+1}}$ and $y = e^{\eta_{i,h}^n}$, we have

$$\frac{\left(e^{\eta_{i,h}^{n+1}}, \eta_{i,h}^{n+1}\right) - \left(e^{\eta_{i,h}^n}, \eta_{i,h}^n\right)}{\tau} + D_i \int_\Omega e^{\eta_{i,h}^n}\left|\nabla \eta_{i,h}^{n+1}\right|^2 + \tau m\hat{\alpha}\int_\Omega \left|e^{\eta_{i,h}^n}\nabla \eta_{i,h}^{n+1}\right|^2 + \frac{\tau m}{2}\beta_i z_i^2 D_i R\int_\Omega \left|e^{\eta_{i,h}^n}\nabla \eta_{i,h}^{n+1}\right|^2$$
$$\le \left(\boldsymbol{u}_h^n, e^{\eta_{i,h}^n}\nabla \eta_{i,h}^{n+1}\right) + \left(\beta_i z_i \boldsymbol{E}_h^n, e^{\eta_{i,h}^n}\nabla \eta_{i,h}^{n+1}\right).$$

Multiplying $\hat{\alpha}$ to the above equation and summing them up for $i = 1, 2, \cdots, m$, we get

$$\frac{1}{\tau}\left(\sum_{i=1}^m \int_\Omega \hat{\alpha} e^{\eta_{i,h}^{n+1}}\eta_{i,h}^{n+1} - \sum_{i=1}^m \int_\Omega \hat{\alpha} e^{\eta_{i,h}^n}\eta_{i,h}^n\right) + \sum_{i=1}^m \hat{\alpha} D_i \int_\Omega e^{\eta_{i,h}^n}\left|\nabla \eta_{i,h}^{n+1}\right|^2$$
$$+ \tau m\hat{\alpha}^2 \sum_{i=1}^m \int_\Omega \left|e^{\eta_{i,h}^n}\nabla \eta_{i,h}^{n+1}\right|^2 + \frac{\tau m}{2}\sum_{i=1}^m R\hat{\alpha}\beta_i z_i^2 D_i R\int_\Omega \left|e^{\eta_{i,h}^n}\nabla \eta_{i,h}^{n+1}\right|^2$$
$$\le \sum_{i=1}^m \hat{\alpha}\left(\boldsymbol{u}_h^n, e^{\eta_{i,h}^n}\nabla \eta_{i,h}^{n+1}\right) + \sum_{i=1}^m \left(\hat{\alpha}\beta_i z_i \boldsymbol{E}_h^n, e^{\eta_{i,h}^n}\nabla \eta_{i,h}^{n+1}\right). \tag{4.7}$$

By taking $\boldsymbol{C}_h = \boldsymbol{B}_h^{n+1}$ in (3.6a), we have

$$\left(\nabla \times \boldsymbol{E}_h^{n+1}, \boldsymbol{B}_h^{n+1}\right) + \epsilon \frac{\left\|\boldsymbol{B}_h^{n+1}\right\|^2 - \left\|\boldsymbol{B}_h^{n}\right\|^2 + \left\|\boldsymbol{B}_h^{n+1} - \boldsymbol{B}_h^{n}\right\|^2}{2\tau} = 0.$$

By taking $\boldsymbol{M}_h = \boldsymbol{E}_h^{n+1}$ in (3.6b), we get

$$\begin{aligned}
&\left(\boldsymbol{B}_h^{n+1}, \nabla \times \boldsymbol{E}_h^{n+1}\right) - \epsilon \frac{\left\|\boldsymbol{E}_h^{n+1}\right\|^2 - \left\|\boldsymbol{E}_h^{n}\right\|^2 + \left\|\boldsymbol{E}_h^{n+1} - \boldsymbol{E}_h^{n}\right\|^2}{2\tau} - \tau\epsilon R\hat{\beta} \left\| \sum_{i=1}^{m} e^{\eta_{i,h}^n} z_i \boldsymbol{E}_h^{n+1} \right\|^2 \\
&= \left(\epsilon R \sum_{i=1}^{m} \left(e^{\eta_{i,h}^n} z_i \boldsymbol{u}_h^n - z_i D_i e^{\eta_{i,h}^n} \nabla \eta_{i,h}^{n+1} + \beta_i e^{\eta_{i,h}^n} z_i^2 \boldsymbol{E}_h^{n+1} \right), \boldsymbol{E}_h^{n+1} \right).
\end{aligned}$$

Summing up the above two equations and multiplying $\hat{\beta}/(\epsilon R)$, we obtain

$$\begin{aligned}
&\frac{\hat{\beta}}{R} \frac{\left\|\boldsymbol{B}_h^{n+1}\right\|^2 - \left\|\boldsymbol{B}_h^{n}\right\|^2 + \left\|\boldsymbol{B}_h^{n+1} - \boldsymbol{B}_h^{n}\right\|^2}{2\tau} + \frac{\hat{\beta}}{R} \frac{\left\|\boldsymbol{E}_h^{n+1}\right\|^2 - \left\|\boldsymbol{E}_h^{n}\right\|^2 + \left\|\boldsymbol{E}_h^{n+1} - \boldsymbol{E}_h^{n}\right\|^2}{2\tau} + \tau\hat{\beta}^2 \left\| \sum_{i=1}^{m} e^{\eta_{i,h}^n} z_i \boldsymbol{E}_h^{n+1} \right\|^2 \\
&= -\sum_{i=1}^{m} \left(\hat{\beta} \left(e^{\eta_{i,h}^n} z_i \boldsymbol{u}_h^n - z_i D_i e^{\eta_{i,h}^n} \nabla \eta_{i,h}^{n+1} + \beta_i e^{\eta_{i,h}^n} z_i^2 \boldsymbol{E}_h^{n+1} \right), \boldsymbol{E}_h^{n+1} \right).
\end{aligned} \tag{4.8}$$

Then, combining (4.6)-(4.8), we have

$$\begin{aligned}
&\frac{\left\|\boldsymbol{u}_h^{n+1}\right\|^2 - \left\|\boldsymbol{u}_h^{n}\right\|^2 + \left\|\boldsymbol{u}_h^{n+1} - \boldsymbol{u}_h^{n}\right\|^2}{2\tau} + \frac{1}{\tau} \left(\sum_{i=1}^{m} \int_\Omega \hat{\alpha} e^{\eta_{i,h}^{n+1}} \eta_{i,h}^{n+1} - \sum_{i=1}^{m} \int_\Omega \hat{\alpha} e^{\eta_{i,h}^{n}} \eta_{i,h}^{n} \right) \\
&+ \frac{\hat{\beta}}{R} \frac{\left\|\boldsymbol{B}_h^{n+1}\right\|^2 - \left\|\boldsymbol{B}_h^{n}\right\|^2 + \left\|\boldsymbol{B}_h^{n+1} - \boldsymbol{B}_h^{n}\right\|^2}{2\tau} + \frac{\hat{\beta}}{R} \frac{\left\|\boldsymbol{E}_h^{n+1}\right\|^2 - \left\|\boldsymbol{E}_h^{n}\right\|^2 + \left\|\boldsymbol{E}_h^{n+1} - \boldsymbol{E}_h^{n}\right\|^2}{2\tau} \\
&+ \tau m \hat{\alpha}^2 \sum_{i=1}^{m} \int_\Omega \left| e^{\eta_{i,h}^n} \nabla \eta_{i,h}^{n+1} \right|^2 + \frac{\tau m}{2} \sum_{i=1}^{m} R \hat{\alpha} \beta_i z_i^2 D_i R \int_\Omega \left| e^{\eta_{i,h}^n} \nabla \eta_{i,h}^{n+1} \right|^2 + \tau\hat{\beta}^2 \left\| \sum_{i=1}^{m} e^{\eta_{i,h}^n} z_i \boldsymbol{E}_h^{n+1} \right\|^2 \\
&\le \sum_{i=1}^{m} \left(\hat{\beta} e^{\eta_{i,h}^n} z_i \boldsymbol{E}_h^{n+1}, \boldsymbol{u}_h^{n+1} - \boldsymbol{u}_h^{n} \right) - \sum_{i=1}^{m} \left(\hat{\alpha} e^{\eta_{i,h}^n} \nabla \eta_{i,h}^{n+1}, \boldsymbol{u}_h^{n+1} - \boldsymbol{u}_h^{n} \right) \\
&\quad + \sum_{i=1}^{m} \left(\hat{\alpha} \beta_i z_i \boldsymbol{E}_h^{n}, e^{\eta_{i,h}^n} \nabla \eta_{i,h}^{n+1} \right) + \sum_{i=1}^{m} \left(\hat{\beta} \left(z_i D_i e^{\eta_{i,h}^n} \nabla \eta_{i,h}^{n+1} - \beta_i e^{\eta_{i,h}^n} z_i^2 \boldsymbol{E}_h^{n+1} \right), \boldsymbol{E}_h^{n+1} \right) \\
&\quad - R_e^{-1} \int_\Omega \left| \nabla \boldsymbol{u}_h^{n+1} \right|^2 - \gamma \int_\Omega \left| \nabla \cdot \boldsymbol{u}_h^{n+1} \right|^2 - \sum_{i=1}^{m} \hat{\alpha} D_i \int_\Omega e^{\eta_{i,h}^n} \left| \nabla \eta_{i,h}^{n+1} \right|^2. \\
&= \sum_{i=1}^{m} (\hat{\beta} e^{\eta_{i,h}^n} z_i \boldsymbol{E}_h^{n+1}, \boldsymbol{u}_h^{n+1} - \boldsymbol{u}_h^{n}) + \sum_{i=1}^{m} \left(\hat{\alpha} e^{\eta_{i,h}^n} \nabla \eta_{i,h}^{n+1}, \boldsymbol{u}_h^{n} - \boldsymbol{u}_h^{n+1} \right) \\
&\quad + \sum_{i=1}^{m} \left(\hat{\beta} D_i z_i \left(\boldsymbol{E}_h^{n} - \boldsymbol{E}_h^{n+1} \right), e^{\eta_{i,h}^n} \nabla \eta_{i,h}^{n+1} \right) - R_e^{-1} \int_\Omega \left| \nabla \boldsymbol{u}_h^{n+1} \right|^2 \\
&\quad - \gamma \int_\Omega \left| \nabla \cdot \boldsymbol{u}_h^{n+1} \right|^2 - \sum_{i=1}^{m} \int_\Omega e^{\eta_{i,h}^n} \left| \sqrt{\hat{\alpha} D_i} \nabla \eta_{i,h}^{n+1} - \sqrt{\hat{\beta} \beta_i} z_i \boldsymbol{E}_h^{n+1} \right|^2,
\end{aligned} \tag{4.9}$$

where we have used the relation $\hat{\alpha}\beta_i = \hat{\beta}D_i$. Using the Cauchy-Schwarz inequality and Young inequality, we derive the first three terms on the right hand side of (4.9) that

$$\sum_{i=1}^{m}\left(\hat{\beta}e^{\eta_{i,h}^n}z_i\boldsymbol{E}_h^{n+1},\boldsymbol{u}_h^{n+1}-\boldsymbol{u}_h^n\right) \le \left\|\boldsymbol{u}_h^{n+1}-\boldsymbol{u}_h^n\right\|\left\|\hat{\beta}\sum_{i=1}^{m}e^{\eta_{i,h}^n}z_i\boldsymbol{E}^{n+1}\right\|$$
$$\le \frac{1}{4\tau}\left\|\boldsymbol{u}_h^{n+1}-\boldsymbol{u}_h^n\right\|^2+\tau\hat{\beta}^2\left\|\sum_{i=1}^{m}e^{\eta_{i,h}^n}z_i\boldsymbol{E}^{n+1}\right\|^2, \tag{4.10}$$

$$\sum_{i=1}^{m}\left(\hat{\alpha}e^{\eta_{i,h}^n}\nabla\eta_{i,h}^{n+1},\boldsymbol{u}_h^n-\boldsymbol{u}_h^{n+1}\right) \le \sum_{i=1}^{m}\left\|\boldsymbol{u}_h^{n+1}-\boldsymbol{u}_h^n\right\|\left\|\hat{\alpha}e^{\eta_{i,h}^n}\nabla\eta_{i,h}^{n+1}\right\|$$
$$\le \frac{1}{4\tau}\left\|\boldsymbol{u}_h^{n+1}-\boldsymbol{u}_h^n\right\|^2+\tau m\hat{\alpha}^2\sum_{i=1}^{m}\left\|e^{\eta_{i,h}^n}\nabla\eta_{i,h}^{n+1}\right\|^2, \tag{4.11}$$

$$\sum_{i=1}^{m}\left(\hat{\beta}D_iz_i\left(\boldsymbol{E}_h^n-\boldsymbol{E}_h^{n+1}\right),e^{\eta_{i,h}^n}\nabla\eta_{i,h}^{n+1}\right) \le \sum_{i=1}^{m}\hat{\beta}D_iz_i\left\|\boldsymbol{E}_h^{n+1}-\boldsymbol{E}_h^n\right\|\left\|e^{\eta_{i,h}^n}\nabla\eta_{i,h}^{n+1}\right\|$$
$$\le \frac{\hat{\beta}}{2\tau R}\left\|\boldsymbol{E}_h^{n+1}-\boldsymbol{E}_h^n\right\|^2+\frac{\tau m\hat{\beta}R}{2}\sum_{i=1}^{m}D_i^2z_i^2\left\|e^{\eta_{i,h}^n}\nabla\eta_{i,h}^{n+1}\right\|^2 \tag{4.12}$$

Plugging (4.10)-(4.12) into (4.9), we get the required estimate (4.5). The proof is thus complete. □

5. Numerical experiments. In this section, we present a series of numerical examples to verify the theoretical results in the previous section. The numerical experiments are implemented on the finite element software Parallel Hierarchical Grid (PHG) [48]. All computations are carried out on the LSSC-IV Cluster of the State Key Laboratory of Scientific and Engineering Computing, Chinese Academy of Sciences. In the numerical experiments, we set

$$\begin{aligned}
S_h &:= \{s_h \in S : s_h|_K \in P_1(K), \quad \forall K \in \mathcal{T}_h\},\\
\boldsymbol{V}_h &:= \{\boldsymbol{v}_h \in \boldsymbol{V} : \boldsymbol{v}_h|_K \in \boldsymbol{P}_{1,b}(K), \quad \forall K \in \mathcal{T}_h\},\\
Q_h &:= \left\{q_h \in H^1(\Omega) : q_h|_K \in P_1(K), \quad \forall K \in \mathcal{T}_h\right\} \cap Q,\\
\boldsymbol{D}_h &:= \{\boldsymbol{C}_h \in \boldsymbol{D} : \boldsymbol{C}_h|_K \in \boldsymbol{P}_0(K) + \boldsymbol{x}P_0(K), \quad \forall K \in \mathcal{T}_h\},\\
\boldsymbol{W}_h &:= \{\boldsymbol{M}_h \in \boldsymbol{W} : \boldsymbol{M}_h|_K \in \boldsymbol{P}_0(K) + \boldsymbol{x} \times \boldsymbol{P}_0(K), \quad \forall K \in \mathcal{T}_h\},
\end{aligned}$$

where $P_{1,b}(K)$ is the set of linear polynomials plus a bubble on K. We use the Newton method to solve the nonlinear system in **Step 1**, and use the PCG and the FGMRES methods to solve the linear systems in **Step 2.1** and **Step 3**, respectively. More implementation details are given in Appendix.

EXAMPLE 5.1 (Accuracy test). *This example is to test the convergence rate for the proposed scheme with a two-component system. In the test, the computational domain is taken as a unit cube $\Omega = (0,1)^3$, the final time of the evolution is taken as $T = 1$ and the physical parameters are set by*

$$R_e = 1, \quad \hat{\alpha} = \hat{\beta} = 1, \quad z_1 = 1, \quad z_2 = -1,$$
$$D_1 = D_2 = \beta_1 = \beta_2 = 1, \quad \epsilon = R = 1.$$

The right-hand sides, initial conditions and the boundary conditions in the model are chosen such that the exact solutions are given by

$$\boldsymbol{u} = -\exp(-t)/2\sin(\pi x)\sin(\pi y)\sin(\pi z)\boldsymbol{\Psi}, \quad p = \exp(-t)(2x-1)(2y-1)(2z-1),$$
$$\boldsymbol{E} = \cos(t)/2\boldsymbol{\Psi}, \quad \boldsymbol{B} = 3\pi\sin(t)/2(-(\cos(\pi x)\sin(\pi y)\sin(\pi z), 0, \cos(\pi z)\sin(\pi x)\sin(\pi y)),$$

$$\eta_1 = \eta_2 = \exp(-t)\cos(\pi x)\cos(\pi y)\cos(\pi z),$$
$$\boldsymbol{\Psi} = (\sin(\pi x)\cos(\pi y)\cos(\pi z), -2\cos(\pi x)\sin(\pi y)\cos(\pi z), \cos(\pi x)\cos(\pi y)\sin(\pi z)).$$

In the numerical test, the initial mesh size and time step are set by $h_0 = \sqrt{3}/4$ and $\tau_0 = 0.05$. We decrease the time step and the mesh size at the same time such that $\tau \propto h$ to test the convergence orders for the proposed scheme. The corresponding numerical errors are displayed in Table 5.1 for the proposed scheme. Here we denote the numerical errors at $t = t_N$ as $\theta_\chi^N = \chi(t_N) - \chi_h^N$ for $\chi = \boldsymbol{u}, p, \eta_i, \boldsymbol{B}, \boldsymbol{E}$. We observe that the errors become smaller and smaller as the mesh size and time step are refined, and the expected first-order convergence rate is obtained asymptotically for all the unknowns. To further test the convergence rates of L^2-errors of $\boldsymbol{u}$, η_1 and η_2, we decrease the time step and the mesh size simultaneously in the scaling of $\tau \propto h^2$. The corresponding results are displayed in Table 5.2, which indicates the expected optimal second convergence rates of the proposed scheme are observed. In addition, from Tables 5.1-5.2, we can see that the magnitudes of $\left\|\mathrm{div}\boldsymbol{B}_h^N\right\|$ are in the order of $10^{-14} \sim 10^{-13}$. This confirms the exactness of the divergence-free condition of $\boldsymbol{B}_h^N$ on the discrete level when neglecting the accumulation of the round-off errors during the computation. This implies that the Gauss's law for the magnetic field holds exactly on the discrete level due to the structure-preserving discretization.

Table 5.1: Errors and convergence rates for the proposed scheme with $\tau \propto h$.

(τ, h)	$\left\|\theta_{\boldsymbol{u}}^N\right\|_1$	$\left\|\theta_p^N\right\|$	$\left\|\theta_{\eta_1}^N\right\|_1$	$\left\|\theta_{\eta_2}^N\right\|_1$
(τ_0, h_0)	2.71e-01(——)	4.71e-01(——)	3.62e-01(——)	3.62e-01(——)
$(\tau_0, h_0)/2$	1.49e-01(0.86)	2.49e-01(0.92)	1.95e-01(0.89)	1.95e-01(0.89)
$(\tau_0, h_0)/4$	7.30e-02(1.03)	1.09e-01(1.19)	1.01e-01(0.95)	1.01e-01(0.95)
$(\tau_0, h_0)/8$	3.58e-02(1.03)	4.08e-02(1.42)	5.11e-02(0.98)	5.11e-02(0.98)
$(\tau_0, h_0)/16$	1.78e-02(1.01)	1.48e-02(1.46)	2.58e-02(0.99)	2.58e-02(0.99)

(τ, h)	$\left\|\theta_{\boldsymbol{E}}^N\right\|$	$\left\|\theta_{\boldsymbol{E}}^N\right\|_{\mathbf{curl}}$	$\left\|\theta_{\boldsymbol{B}}^N\right\|$	$\left\|\nabla \cdot \boldsymbol{B}_h^N\right\|$
(τ_0, h_0)	7.69e-02(——)	4.50e-01(——)	6.77e-01(——)	1.02e-14
$(\tau_0, h_0)/2$	4.01e-02(0.94)	2.32e-01(0.96)	3.47e-01(0.97)	2.36e-14
$(\tau_0, h_0)/4$	2.07e-02(0.96)	1.17e-01(0.99)	1.74e-01(0.99)	4.93e-14
$(\tau_0, h_0)/8$	1.05e-02(0.97)	5.88e-02(0.99)	8.73e-02(1.00)	1.11e-13
$(\tau_0, h_0)/16$	5.33e-03(0.98)	2.95e-02(1.00)	4.37e-02(1.00)	2.72e-13

Table 5.2: Errors and convergence rates for the proposed scheme with $\tau \propto h^2$.

(τ, h)	$\left\|\theta_{\boldsymbol{u}}^N\right\|$	$\left\|\theta_{\eta_1}^N\right\|$	$\left\|\theta_{\eta_2}^N\right\|$	$\left\|\nabla \cdot \boldsymbol{B}_h^N\right\|$
(τ_0, h_0)	2.63e-02(——)	5.30e-02(——)	5.31e-02(——)	1.02e-14
$(\tau_0/4, h_0/2)$	8.50e-03(1.63)	1.67e-02(1.66)	1.67e-02(1.66)	2.42e-14
$(\tau_0/16, h_0/4)$	2.07e-03(2.04)	4.47e-03(1.90)	4.47e-03(1.90)	6.62e-14
$(\tau_0/64, h_0/8)$	4.88e-04(2.08)	1.14e-03(1.98)	1.14e-03(1.98)	2.27e-13
$(\tau_0/256, h_0/16)$	1.18e-04(2.05)	2.85e-04(1.99)	2.85e-04(1.99)	8.53e-13

To study the performance of the proposed solver, we further present the number of nonlinear and linear iterations for each step in the algorithm with $\tau \propto h$ at $t = T$ in Table 5.3. As for the nonlinear iterations, we find that the number of Newton iterations is almost the same and quite small. Thus, for this test, the Newton

method enjoys the pretty good convergence. As for the linear iterations, there is no significant difference on the numbers of iterations. This exhibits good performance of the proposed solver for the algebraic system.

Table 5.3: Numbers of nonlinear iterations and linear iterations at $t = T$.

(τ, h)	**Step 1**		**Step 2.1**	**Step 3**
	Solver for η_1	Solver for η_2	N_{pcg}	N_{fgmres}
	$N_{\text{newton}}(N_{\text{pcg}}^{\text{average}})$	$N_{\text{newton}}(N_{\text{pcg}}^{\text{average}})$		
(τ_0, h_0)	10(12)	10(12)	8	27
$(\tau_0, h_0)/2$	7(10)	7(10)	8	33
$(\tau_0, h_0)/4$	5(9)	5(9)	8	33
$(\tau_0, h_0)/8$	3(9)	3(9)	8	33
$(\tau_0, h_0)/16$	2(10)	2(10)	8	32

EXAMPLE 5.2 (Physics preserving properties test). *This example is to investigate the unconditional energy stability, magnetic-flux-conservation and mass-conservation properties of the proposed scheme with a three-component system. We take the domain as* $\Omega = (0,1)^3$ *and set the initial conditions for* $\boldsymbol{u}$, η_i, $\boldsymbol{B}$ *and* $\boldsymbol{E}$ *to be*

$$\begin{aligned}
&\boldsymbol{u}^0 = -1/2 \sin(\pi x) \sin(\pi y) \sin(\pi z)\, \boldsymbol{\Psi}, \quad \boldsymbol{B}^0 = \boldsymbol{0}, \quad \boldsymbol{E}^0 = -1/2\boldsymbol{\Psi},\\
&\eta_1^0 = \eta_2^0 = \eta_3^0 = \cos(\pi x)\cos(\pi y)\cos(\pi z),\\
&\boldsymbol{\Psi} = (\sin(\pi x)\cos(\pi y)\cos(\pi z), -2\cos(\pi x)\sin(\pi y)\cos(\pi z), \cos(\pi x)\cos(\pi y)\sin(\pi z)).
\end{aligned}$$

Moreover, the final time is given by $T = 2$.

With the given data, we test the properties under different physical parameters and time steps on a fixed mesh with $h = \sqrt{3}/16$. Here, the physical number are taken as

$$\begin{aligned}
&R_e = 100, \quad \hat{\alpha} = \hat{\beta} = 1, \quad z_1 = 1, \quad z_2 = 1, \quad z_3 = -2\\
&D_1 = D_2 = D_3 = \beta_1 = \beta_2 = \beta_3 = 0.1, \quad \epsilon = 0.01, \quad R = 1.
\end{aligned}$$

We carry out the numerical tests under different physical parameters and time steps. Figure 5.1 show the time evolution of the total energy, the L^2-norm for $\text{div}\boldsymbol{B}_h^n$ and the mass for the three ions computed by our numerical method. As for the energy stability, we can see that all energy curves decrease monotonically, which means that the proposed scheme is unconditionally energy stable. As for the magnetic flux conservation, $\|\text{div}\boldsymbol{B}_h^n\|$ stays at order of $10^{-15} \sim 10^{-14}$, which verifies the exactness of the divergence-free condition on the discrete level again. As for the mass conservation, all the mass for the ion 1 ($M_{1,h}$), for the ion 2 ($M_{2,h}$) and for the ion 3 ($M_{3,h}$) remain constants. This confirms the scheme is mass-conservative.

EXAMPLE 5.3 (Ion spreading in a charged reservoir.). *This example is to simulate the phenomenon of electron-diffusion of ions in a charged reservoir. In the setting, we consider the flow with two species in a cuboid micro-channel,* $\Omega = (0,1) \times (0,1) \times (0,2)$, *under the external electric field* $\boldsymbol{E}_b = (0,0,1)$. *The boundary conditions on all sides are no-slip, impenetrable and insulating for* $\boldsymbol{u}$, η_i *and* $\boldsymbol{B}$. *As for the initial conditions, we consider an initial state where a Gaussian concentration profile of negatively charged species is placed above and to the right, and the same profile of positively charged species is placed below and to the left of the center of the micro-channel. Specifically, the initial velocity and magnetic field are set as zero, the initial electric field is chosen as* $\boldsymbol{E}_b$ *and the initial concentrations of positively and negatively charged particles are as follows,*

$$\eta_1^0 = \log\left(\frac{C_0}{2\pi R_*^2}\exp\left(-\frac{(x - L_x/2 + l_x)^2 + (y - L_y/2 + l_y)^2 + (z - L_z/2 + l_z)^2}{2R_*^2}\right)\right),$$

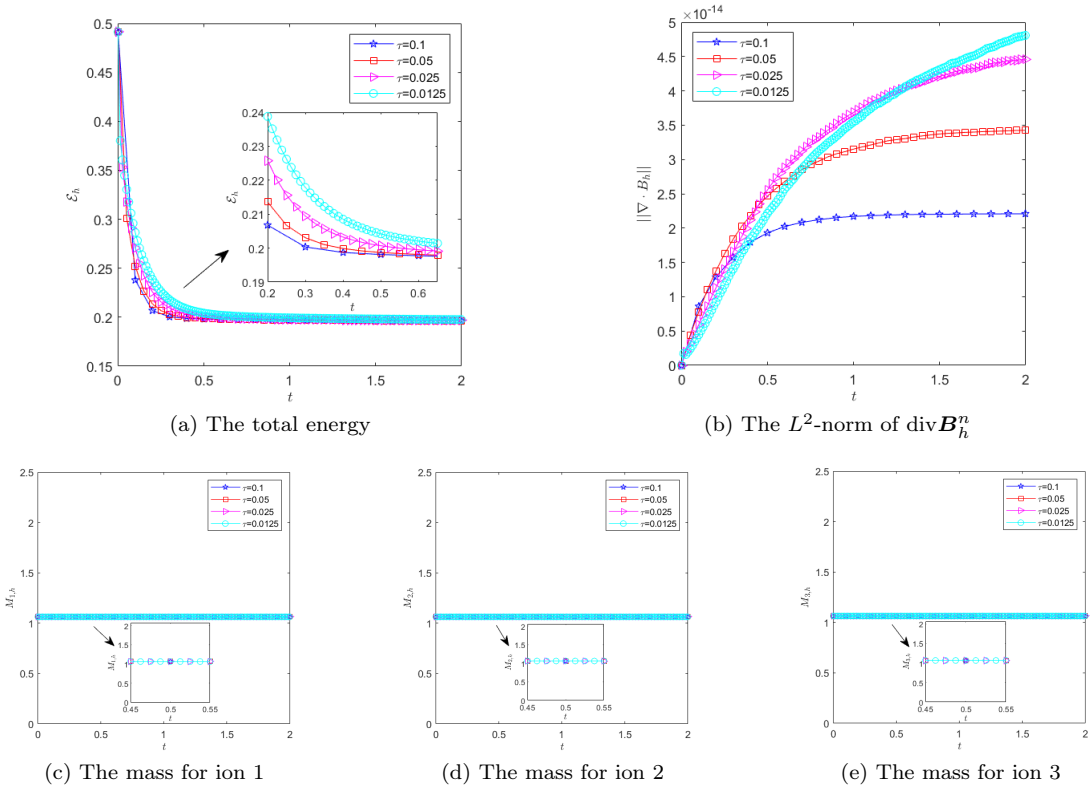

(a) The total energy

(b) The L^2-norm of $\mathrm{div}\boldsymbol{B}_h^n$

(c) The mass for ion 1

(d) The mass for ion 2

(e) The mass for ion 3

Fig. 5.1: Time evolution of some quantities with different time steps.

$$\eta_2^0 = \log\left(\frac{C_0}{2\pi R_*^2}\exp\left(-\frac{(x-L_x/2-l_x)^2+(y-L_y/2-l_y)^2+(z-L_z/2-l_z)^2}{2R_*^2}\right)\right),$$

where the parameters are given by $C_0 = 3$, $R_* = 0.25$, $L_x = L_y = 1$, $L_z = 2$, $l_x = l_y = 0.125$ *and* $l_z = 0.25$. *Moreover, the physical parameters are given by*

$$R_e = 100, \quad \hat{\alpha} = 0.2, \quad \hat{\beta} = 2, \quad z_1 = 1, \quad z_2 = -1,$$
$$D_1 = D_2 = 0.01, \quad \beta_1 = \beta_2 = 0.1, \quad \epsilon = 0.01, \quad R = 0.5.$$

Here, we use a regular and uniform tetrahedral mesh with the grid size $h = \sqrt{3}/32$, which consists of 393216 elements, 2875270 degrees of freedom in total. Then we conduct the simulations with the time step $\tau = 0.005$ until the final time $T = 2.5$ is reached. To investigate visually how the system evolutes, we display snapshots on the cross section $x = 0.5$ at some time instants of the net charge in Figure 5.2, the streamlines of the fluid velocity in Figure 5.3, the distributions of the electric field and magnetic field in Figures 5.4-5.5. Note that our results in Figures 5.2-5.3 are similar to the previous results in [32], which studied the Navier-Stokes-Poisson-Nernst-Planck model. The similarity is due to the fact that the magnetic field is relatively small in this case (see Figure 5.5). As we can see, since the external electric field impels the ions towards opposite ends of the reservoir, while the positive and negative charges are pulled towards each other, the flow occurs and then decays due to dissipation. We also find the total electric field is almost equal to the applied electric field at the very beginning and then the total electric field gradually deviates the external imposed electric field because of the enhanced induced electric field.

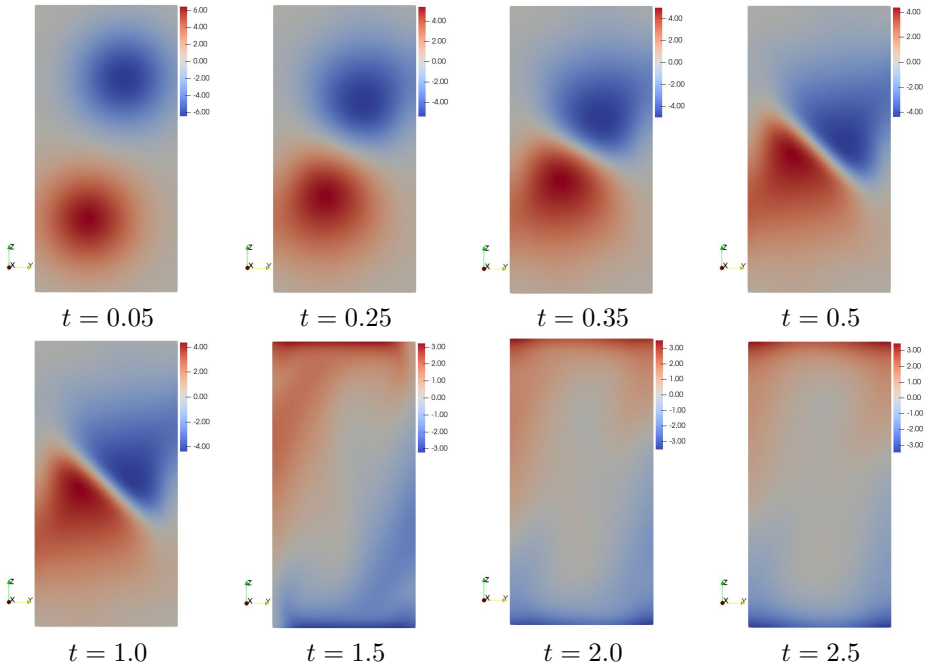

Fig. 5.2: Snapshots in time of the net charge on the cross section $x = 0.5$ with $\boldsymbol{E}_b = (0, 0, 1)$.

EXAMPLE 5.4 (Electro-convection flow subjected to charge injection.). *In this example, we investigate the electro-convection phenomena subjected to charge injection. The computational domain is a cuboid,* $\Omega = (0, 5) \times (0, 1) \times (0, 1)$ *and the external electric field is set by* $\boldsymbol{E}_b = (0, 0, 1)$. *The boundary conditions are given as*

$$\begin{aligned} \boldsymbol{u} = \boldsymbol{0}, \quad \boldsymbol{B} \times \boldsymbol{n} = \boldsymbol{0} \quad & on \quad \Gamma, \\ \eta_1 = \log 6, \quad \eta_2 = \log 1 \quad & on \quad \Gamma_D, \\ (-D_i \nabla \eta_i + \boldsymbol{u} + \beta_i z_i \boldsymbol{E}) \cdot \boldsymbol{n} = 0 \quad & on \quad \Gamma_N, \end{aligned}$$

where $\Gamma_D = \{(x, y, 1) : 0 \le x \le 5,\ 0 \le y \le 1, \}$ *and* $\Gamma_N = \Gamma \backslash \Gamma_D$. *The initial velocity and magnetic field are set as zero, the initial electric field is chosen as* $\boldsymbol{E}_b$, *and the initial concentrations of positive and negative charged particles are given by* $\eta_1^0 = \eta_2^0 = \log 1$. *Furthermore, the physical parameters are given by*

$$\begin{aligned} &R_e = 300, \quad \hat{\alpha} = 2.0, \quad \hat{\beta} = 10.0, \quad z_1 = 1, \quad z_2 = -1, \\ &D_1 = D_2 = 0.01, \quad \beta_1 = \beta_2 = 0.05, \quad \epsilon = 0.01, \quad R = 0.25. \end{aligned}$$

In the simulation, the mesh size, time step and final time are set as $h = \sqrt{3}/16$, $\tau = 0.005$ and $T = 30$, respectively. Figure 5.6 presents some snapshots on the cross section $y = 0.5$ at some time instants of the streamlines of the fluid velocity. We find that a series of symmetric vortexes are gradually formed from the left and right sides of the domain, and exhibits multiple cell-structures finally. These results are in a good agreement with [44, 47].

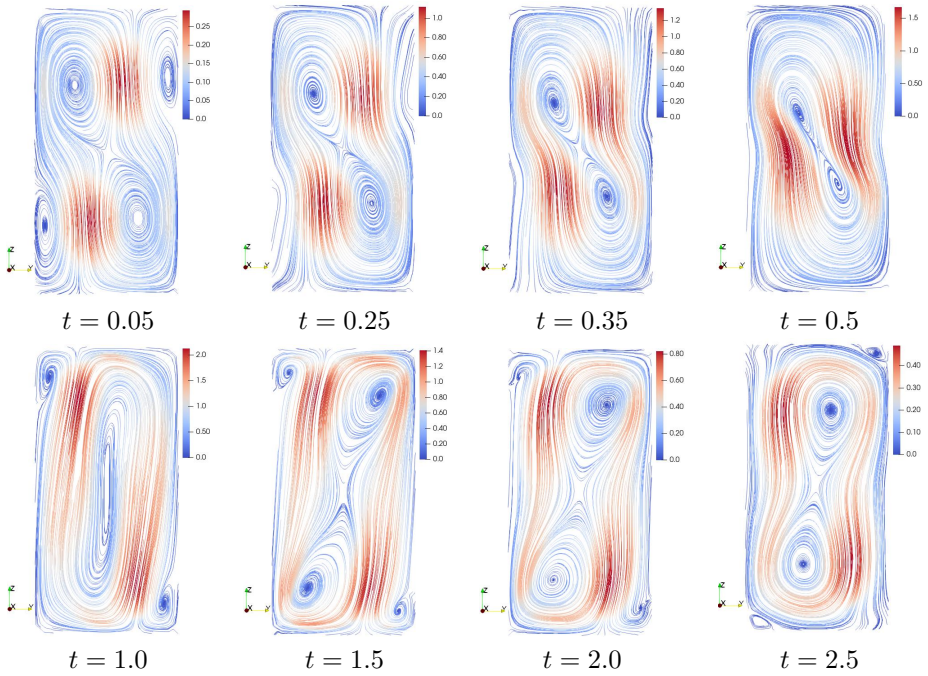

Fig. 5.3: Snapshots in time of streamlines of $\boldsymbol{u}_h^n$ on the cross section $x = 0.5$ with $\boldsymbol{E}_b = (0, 0, 1)$.

6. Conclusion. In conclusion, we present a new mathematical model and a novel physics-preserving numerical scheme for ion transport in viscous liquid solutions under the influence of electromagnetic fields. The model is represented as a coupled system of the Navier-Stokes, Nernst-Planck, and Maxwell equations. We first establish several key properties of the continuous model, including the positivity and conservation of ion concentration, the preservation of magnetic flux, and the structure of energy dissipation. Notably, we demonstrate that retaining a gradient term for ion concentrations in the Navier-Stokes equations is crucial for designing an energy-stable numerical scheme using standard finite element spaces. Typically, this gradient term is absorbed into the pressure term in the conventional Navier-Stokes-Poisson-Nernst-Planck systems found in the literature. We then develop a decoupled, fully discrete numerical scheme by integrating various numerical techniques. These include applying a logarithmic transformation to the ion concentrations, employing innovative implicit-explicit treatments for the nonlinear coupling terms, introducing additional stabilization terms, and utilizing structure-preserving finite element pairs. In our algorithm, we sequentially solve the Nernst-Planck equation, the Maxwell equation, and the Navier-Stokes equation. Importantly, the concentration of each ion can be solved separately and in parallel, while the electric and magnetic fields are also decoupled. Consequently, our method is highly efficient for solving the coupled Navier-Stokes-Nernst-Planck-Maxwell system. Since we utilize standard finite element spaces for both the Maxwell and Navier-Stokes equations, our algorithm can be implemented in various standard open-source software. Finally, we prove that the fully discrete scheme preserves positivity, conserves mass, maintains magnetic flux, and is unconditionally energy stable. We also conduct numerical simulations to validate the effectiveness of the proposed scheme and the theoretical results. We note that the numerical techniques introduced in this work are novel and applicable even to the standard Navier-Stokes-Poisson-Nernst-Planck system, which is simpler than the model considered in this work. Future work will focus on designing high-order temporal schemes and conducting rigorous error analysis of the proposed scheme.

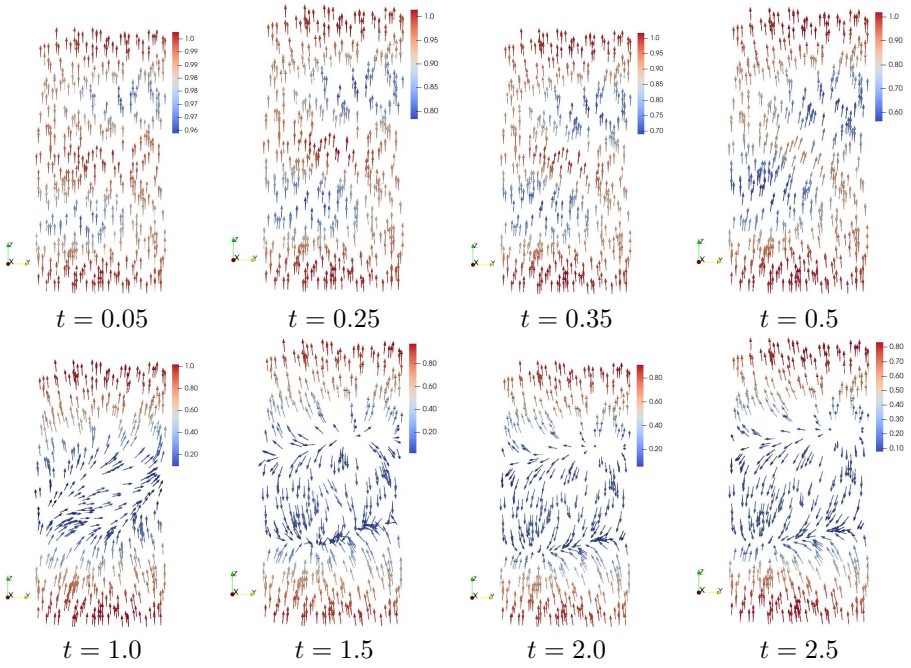

Fig. 5.4: Snapshots in time of distributions of $\boldsymbol{E}_h^n$ on the cross section $x = 0.5$ with $\boldsymbol{E}_b = (0, 0, 1)$.

Appendix. We give some implementation details of the decoupled scheme **Algorithm 1**. First of all, note that **Step 1** still needs to solve a nonlinear system at each time step, we adopt the Newton method to solve it. Define the residuals as

$$\mathcal{R}_i^{n+1,k}\left(\eta_{i,h}^{n+1,k}\right) := \left(\frac{e^{\eta_{i,h}^{n+1,k}} - e^{\eta_{i,h}^n}}{\tau}, s_h\right) - \left(\boldsymbol{u}_h^n e^{\eta_{i,h}^{n,k}}, \nabla s_h\right) + \left(D_i e^{\eta_{i,h}^n} \nabla \eta_{i,h}^{n+1,k}, \nabla s_h\right) - \left(\beta_i e^{\eta_{i,h}^n} z_i \boldsymbol{E}_h^n, \nabla s_h\right)$$
$$+ \frac{\tau m}{2}\left(\beta_i z_i^2 D_i Re^{\eta_{i,h}^n} \nabla \eta_{i,h}^{n+1,k}, e^{\eta_{i,h}^n} \nabla s_h\right) + \tau m\left(\hat{\alpha} e^{\eta_{i,h}^{n,k}} \nabla \eta_{i,h}^{n+1,k}, e^{\eta_{i,h}^{n,k}} \nabla s_h\right),$$

for $i = 1, 2, \cdots, m$, and any $s_h \in S_h$. The purpose of the solver is to compute $\eta_{i,h}^{n+1,k} \in S_h$ such that $\mathcal{R}_i^{n+1,k}\left(\eta_{i,h}^{n+1,k}\right)$ is zero for $i = 1, \cdots, m$. To solve the residual equation, the problem must be linearized, the Frechét derivatives of the residuals are

$$\mathcal{J}_i^{n+1,k}\left(\eta_{i,h}^{n+1,k}\right)\left[\delta\eta_{i,h}^{n+1,k}\right] = \frac{1}{\tau}\left(e^{\eta_{i,h}^{n+1,k}} \delta\eta_{i,h}^{n+1,k}, s_h\right) + \left(D_i e^{\eta_{i,h}^n} \nabla \delta\eta_{i,h}^{n+1,k}, \nabla s_h\right)$$
$$+ \tau m\left(\hat{\alpha} e^{\eta_{i,h}^{n,k}} \nabla \delta\eta_{i,h}^{n+1,k}, e^{\eta_{i,h}^{n,k}} \nabla s_h\right) + \frac{\tau m}{2}\left(\beta_i z_i^2 D_i Re^{\eta_{i,h}^n} \nabla \delta\eta_{i,h}^{n+1,k}, e^{\eta_{i,h}^n} \nabla s_h\right),$$

for $i = 1, 2, \cdots, m$. It is clear that the Frechét derivatives are linear operators of $\delta\eta_{i,h}^{n+1,k}$. Given an initial guess, $\eta_{i,h}^{n+1,0}$, that satisfies the boundary conditions, the solution to the residual equations is computed by the sequence of approximate solutions defined by solving for $\delta\eta_{i,h}^{n+1,k} \in S_h$ such that

$$\mathcal{J}_i^{n+1,k}\left(\eta_{i,h}^{n+1,k}\right)\left[\delta\eta_{i,h}^{n+1,k}\right] = -\mathcal{R}_i^{n+1}\left(\eta_{i,h}^{n+1,k}\right),$$

for $i = 1, \cdots, N$, and updating with some damping factor $0 < \mu \leq 1$,

$$\eta_{i,h}^{n+1,k+1} \leftarrow \eta_{i,h}^{n+1,k} + \mu\delta\eta_{i,h}^{n+1,k}.$$

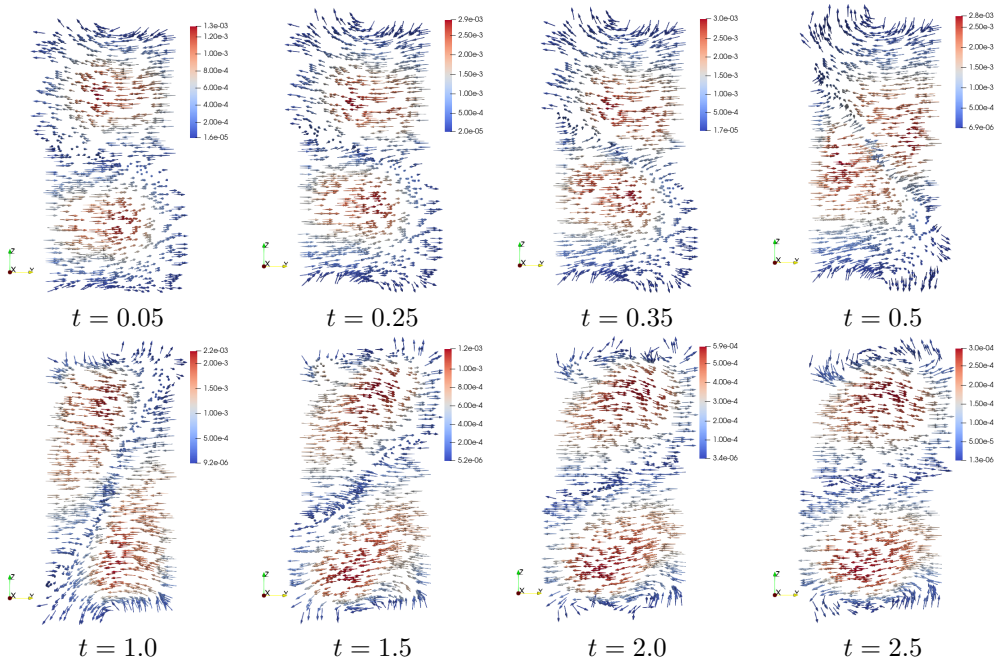

Fig. 5.5: Snapshots in time of distributions of $\boldsymbol{B}_h^n$ on the cross section $x = 0.5$ with $\boldsymbol{E}_b = (0, 0, 1)$.

Since the previous value $\eta_{i,h}^n$ provides a good initial value, the Newton solver only takes a few steps to converge. Moreover, to solve the linear system at each iteration, we use the algebraic multigrid method (AMG) preconditioned conjugate gradient method (PCG). The tolerance and maximum iterations for the Newton method are set as $\epsilon_{\text{newton}} = 1\text{e}-9$ and $N_{\text{newton}}^{\max} = 100$. The relative tolerance and maximum iterations for the PCG method are set as $\epsilon_{\text{pcg}}^1 = 1\text{e}-9$ and $N_{\text{pcg},1}^{\max} = 100$. Being different from the scheme developed in [7], the degrees of freedom for all the ion concentrations are decoupled, thus the nonlinear solver and linear solver can be easily constructed. Next, in **Step 2.1**, we need to solve a $\boldsymbol{H}(\mathbf{curl})$-elliptic problem in (3.10) at each time step. Thus, we employ the PCG method with Hiptmair-Xu preconditioner [24], relative tolerance $\epsilon_{\text{pcg}}^2 = 1\text{e}-9$ and maximum iterations $N_{\text{pcg},2}^{\max} = 100$. Finally, **Step 3** requires solving a discrete system with saddle-point structure at each time step. To solve it efficiently, we adopted the augmented Lagrangian block preconditioner [30] preconditioned flexible generalized minimal residual method (FGMRES). The relative tolerance and maximum iterations for the FGMRES method are set as $\epsilon_{\text{gmres}}^2 = 1\text{e}-9$ and $N_{\text{gmres}}^{\max} = 100$. We refer to [29, 30] for the details on the preconditioner.

REFERENCES

[1] H. Akiyama, Y. Shimizu, H. Miyakawa, and M. Inoue, *Extracellular dc electric fields induce nonuniform membrane polarization in rat hippocampal CA1 pyramidal neurons*, Brain research, 1383 (2011), pp. 22–35.

[2] N. R. Aluru, F. Aydin, M. Z. Bazant, D. Blankschtein, A. H. Brozena, J. P. de Souza, M. Elimelech, S. Faucher, J. T. Fourkas, V. B. Koman, et al., *Fluids and electrolytes under confinement in single-digit nanopores*, Chemical reviews, 123 (2023), pp. 2737–2831.

[3] D. Arsénio and I. Gallagher, *Solutions of Navier–Stokes–Maxwell systems in large energy spaces*, Transactions of the American Mathematical Society, 373 (2020), pp. 3853–3884.

[4] D. Arsénio, S. Ibrahim, and N. Masmoudi, *A derivation of the magnetohydrodynamic system from Navier–Stokes–Maxwell systems*, Archive for Rational Mechanics and Analysis, 216 (2015), pp. 767–812.

[5] F. Bertagna, R. Lewis, S. R. P. Silva, J. McFadden, and K. Jeevaratnam, *Effects of electromagnetic fields on*

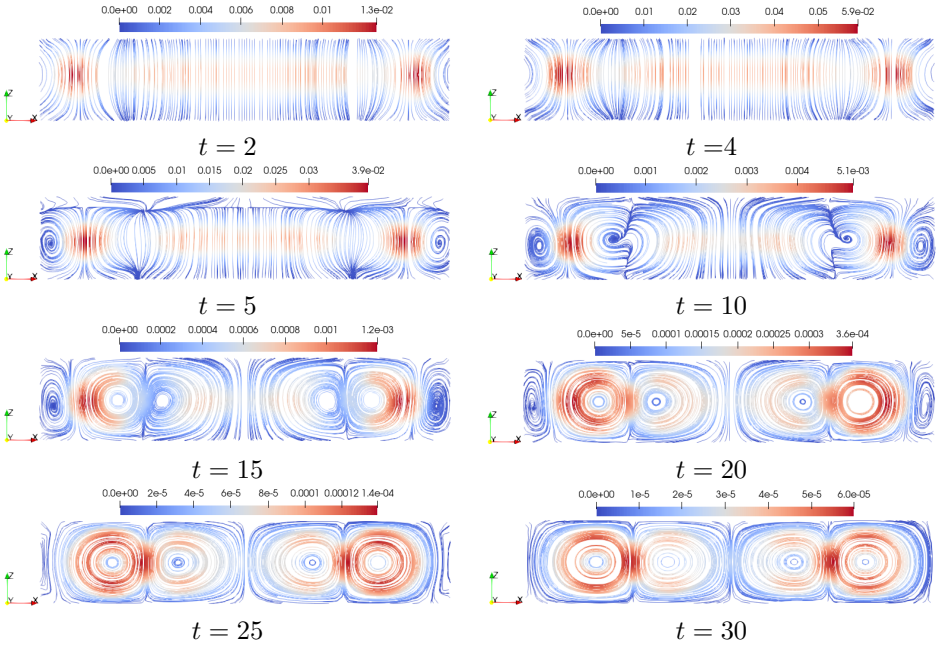

Fig. 5.6: Snapshots in time of streamlines of $\boldsymbol{u}_h^n$ on the cross section $y = 0.5$ with the cuboid domain.

neuronal ion channels: a systematic review, Annals of the New York Academy of Sciences, 1499 (2021), pp. 82–103.

[6] D. Boffi, F. Brezzi, and M. Fortin, *Mixed finite element methods and applications*, vol. 44 of Springer Series in Computational Mathematics, Springer, Heidelberg, 2013.

[7] A. Bousquet, X. Hu, M. S. Metti, and J. Xu, *Newton solvers for drift-diffusion and electrokinetic equations*, SIAM J. Sci. Comput., 40 (2018), pp. B982–B1006.

[8] P. Constantin and M. Ignatova, *On the Nernst–Planck–Navier–Stokes system*, Archive for Rational Mechanics and Analysis, 232 (2019), pp. 1379–1428.

[9] P. Constantin, M. Ignatova, and F.-N. Lee, *Nernst–Planck–Navier–Stokes systems far from equilibrium*, Archive for Rational Mechanics and Analysis, 240 (2021), pp. 1147–1168.

[10] C. I. Correa, G. N. Gatica, and R. Ruiz-Baier, *New mixed finite element methods for the coupled Stokes and Poisson–Nernst–Planck equations in banach spaces*, ESAIM: Mathematical Modelling and Numerical Analysis, 57 (2023), pp. 1511–1551.

[11] J. de Frutos, B. García-Archilla, V. John, and J. Novo, *Analysis of the grad-div stabilization for the time-dependent Navier-Stokes equations with inf-sup stable finite elements*, Adv. Comput. Math., 44 (2018), pp. 195–225.

[12] M. W. de Groot, M. D. Kock, and R. H. Westerink, *Assessment of the neurotoxic potential of exposure to 50 Hz extremely low frequency electromagnetic fields (elf-emf) in naive and chemically stressed pc12 cells*, Neurotoxicology, 44 (2014), pp. 358–364.

[13] M. Dehghan, Z. Gharibi, and R. Ruiz-Baier, *Optimal error estimates of coupled and divergence-free virtual element methods for the Poisson-Nernst-Planck/Navier-Stokes equations and applications in electrochemical systems*, J. Sci. Comput., 94 (2023), pp. 72, 50.

[14] W. E and J.-G. Liu, *Gauge method for viscous incompressible flows*, Commun. Math. Sci., 1 (2003), pp. 317–332.

[15] M. Feychting, A. Ahlbom, and L. Kheifets, *EMF and health*, Annu. Rev. Public Health, 26 (2005), pp. 165–189.

[16] H. Gajewski and K. Gröger, *On the basic equations for carrier transport in semiconductors*, J. Math. Anal. Appl., 113 (1986), pp. 12–35.

[17] P. Germain, S. Ibrahim, and N. Masmoudi, *Well-posedness of the Navier–Stokes–Maxwell equations*, Proceedings of the Royal Society of Edinburgh Section A: Mathematics, 144 (2014), pp. 71–86.

[18] D. Gilbarg and N. S. Trudinger, *Elliptic partial differential equations of second order*, Classics in Mathematics, Springer-Verlag, Berlin, 2001. Reprint of the 1998 edition.

[19] V. Girault and P.-A. Raviart, *Finite element methods for Navier-Stokes equations*, vol. 5 of Springer Series in Computational Mathematics, Springer-Verlag, Berlin, 1986. Theory and algorithms.

[20] P. D. Grossman and J. C. Colburn, *Capillary electrophoresis: Theory and practice*, Academic Press, 2012.

[21] J. L. Guermond, P. Minev, and J. Shen, *An overview of projection methods for incompressible flows*, Comput. Methods Appl. Mech. Engrg., 195 (2006), pp. 6011–6045.
[22] M. He and P. Sun, *Mixed finite element method for modified Poisson–Nernst–Planck/Navier–Stokes equations*, Journal of Scientific Computing, 87 (2021), pp. 1–33.
[23] Y. He and H. Chen, *Efficiently high-order time-stepping R-GSAV schemes for the Navier–Stokes-Poisson-Nernst–Planck equations*, Physica D: Nonlinear Phenomena, (2024), p. 134233.
[24] R. Hiptmair and J. Xu, *Nodal auxiliary space preconditioning in* $\mathbf{H}(\mathbf{curl})$ *and* $\mathbf{H}(\mathrm{div})$ *spaces*, SIAM J. Numer. Anal., 45 (2007), pp. 2483–2509.
[25] Z.-H. Hu, W.-P. Lv, D.-X. Hui, X.-J. Wang, and Y.-N. Wang, *Permeability enhancement of the KcsA channel under radiation of a terahertz wave*, Physical Review E, 105 (2022), p. 024104.
[26] V. John, *Finite element methods for incompressible flow problems*, vol. 51 of Springer Series in Computational Mathematics, Springer, Cham, 2016.
[27] N. Kavokine, R. R. Netz, and L. Bocquet, *Fluids at the nanoscale: from continuum to subcontinuum transport*, Annual Review of Fluid Mechanics, 53 (2021), pp. 377–410.
[28] J. H. Kim, Y. H. Huh, and H. R. Kim, *Trafficking of synaptic vesicles is changed at the hypothalamus by exposure to an 835 MHz radiofrequency electromagnetic field.*, General Physiology & Biophysics, 38 (2019).
[29] L. Li, *Finite element methods and fast solvers for incompressible magetohydrodynamic systems*, PhD thesis, AMSS, Chinese Academy of Sciences, 2018.
[30] L. Li, M. Ni, and W. Zheng, *A charge-conservative finite element method for inductionless MHD equations. Part II: A robust solver*, SIAM J. Sci. Comput., 41 (2019), pp. B816–B842.
[31] Y. Li, C. Chang, Z. Zhu, L. Sun, and C. Fan, *Terahertz wave enhances permeability of the voltage-gated calcium channel*, Journal of the American Chemical Society, 143 (2021), pp. 4311–4318.
[32] G. Linga, A. Bolet, and J. Mathiesen, *Transient electrohydrodynamic flow with concentration-dependent fluid properties: modelling and energy-stable numerical schemes*, J. Comput. Phys., 412 (2020), pp. 109430, 34.
[33] M. S. Metti, J. Xu, and C. Liu, *Energetically stable discretizations for charge transport and electrokinetic models*, J. Comput. Phys., 306 (2016), pp. 1–18.
[34] P. Monk, *Finite element methods for Maxwell's equations*, Numerical Mathematics and Scientific Computation, Oxford University Press, New York, 2003.
[35] W. Peng, Z. Zhu, J. Lou, K. Chen, Y. Wu, and C. Chang, *High-frequency terahertz waves disrupt Alzheimer's β-amyloid fibril formation*, eLight, 3 (2023), p. 18.
[36] A. Prohl and M. Schmuck, *Convergent finite element discretizations of the Navier-Stokes-Nernst-Planck-Poisson system*, ESAIM: Mathematical Modelling and Numerical Analysis, 44 (2010), pp. 531–571.
[37] Z. Qiao, Z. Xu, Q. Yin, and S. Zhou, *A Maxwell-Ampère Nernst-Planck framework for modeling charge dynamics*, SIAM J. Appl. Math., 83 (2023), pp. 374–393.
[38] Z. Qiao, Z. Xu, Q. Yin, and S. Zhou, *Structure-preserving numerical method for Maxwell-Ampère Nernst-Planck model*, J. Comput. Phys., 475 (2023), pp. 111845, 20.
[39] Z. Qiao, Z. Xu, Q. Yin, and S. Zhou, *Local Structure-Preserving Relaxation Method for Equilibrium of Charged Systems on Unstructured Meshes*, SIAM J. Sci. Comput., 46 (2024), pp. A2248–A2269.
[40] M. Schmuck, *Analysis of the Navier–Stokes–Nernst–Planck–Poisson system*, Mathematical Models and Methods in Applied Sciences, 19 (2009), pp. 993–1014.
[41] J. Shen, *Modeling and numerical approximation of two-phase incompressible flows by a phase-field approach*, in Multiscale modeling and analysis for materials simulation, vol. 22 of Lect. Notes Ser. Inst. Math. Sci. Natl. Univ. Singap., World Sci. Publ., Hackensack, NJ, 2012, pp. 147–195.
[42] J. Shen and X. Yang, *Decoupled, energy stable schemes for phase-field models of two-phase incompressible flows*, SIAM J. Numer. Anal., 53 (2015), pp. 279–296.
[43] R. J. Thompson, A. Wilson, T. Moeller, and C. L. Merkle, *A strong conservative Riemann solver for the solution of the coupled Maxwell and Navier–Stokes equations*, Journal of Computational Physics, 258 (2014), pp. 431–450.
[44] P. Traoré and A. T. Pérez, *Two-dimensional numerical analysis of electroconvection in a dielectric liquid subjected to strong unipolar injection*, Physics of Fluids, 24 (2012), p. 037102.
[45] C. Wang and J.-G. Liu, *Convergence of gauge method for incompressible flow*, Math. Comp., 69 (2000), pp. 1385–1407.
[46] Y. Wang, C. Liu, and Z. Tan, *A generalized Poisson–Nernst–Planck–Navier–Stokes model on the fluid with the crowded charged particles: Derivation and its well-posedness*, SIAM Journal on Mathematical Analysis, 48 (2016), pp. 3191–3235.
[47] H. Yao, C. Xu, and M. Azaiez, *Stable and decoupled schemes for an electrohydrodynamics model*, Math. Comput. Simulation, 206 (2023), pp. 689–708.
[48] L.-B. Zhang, *A parallel algorithm for adaptive local refinement of tetrahedral meshes using bisection*, Numer. Math. Theory Methods Appl., 2 (2009), pp. 65–89.